J Mater Sci (2017) 52:13319–13349

Review

Mechanical performance of particulate-reinforced Al metal-matrix composites (MMCs) and Al metal-matrix nano-composites (MMNCs)

Chang-Soo Kim[1,*], Kyu Cho[2], Mohsen H. Manjili[1], and Marjan Nezafati[1]

[1] *Materials Science and Engineering Department, University of Wisconsin-Milwaukee, Milwaukee, WI 53211, USA*
[2] *U.S. Army Research Laboratory, Weapons and Materials Research Directorate, Aberdeen Proving Ground, Aberdeen, MD 21005, USA*

Received: 16 March 2017
Accepted: 10 July 2017
Published online: 17 July 2017

ABSTRACT

The metal-matrix composites/nano-composites (MMCs/MMNCs) reinforced with hard ceramic particulates have received a tremendous attention due to their potential improvements in physical and mechanical performances. In the present work, we have comprehensively collected currently available experimental data sets of Al-based MMCs/MMNCs and have carried out thorough analyses to quantitatively address the impacts of the reinforcement volume fractions, reinforcement particle sizes, and metal-matrix grain sizes on their mechanical properties including the yield strength, ultimate strength, and strain to failure of composites. We also performed a quantitative analysis on the strengthening mechanisms of Al MMNCs to reveal that the grain refinement can play a major role in increasing the strength of composites. Al-based MMC or MMNC materials generally exhibited an indirect relationship between the strength increase and strain-to-failure increase. The results include a critical comparison for the mechanical performance of particulate-reinforced composites for both pure and alloyed Al matrices to elucidate the contemporary status of Al MMC and MMNC materials.

Introduction

The metal-matrix composites reinforced with micron- and nano-sized particulates (MMC and MMNC, respectively) are recognized as one of the attractive advanced materials for various structural applications. Hard ceramic reinforcement materials (oxides, carbides, borides, etc.) are routinely incorporated into these MMCs/MMNCs due to their high strength and stiffness/modulus at both the ambient and elevated temperatures [1–3]. Different from the classical MMC, MMNCs are generally referred to as the composites containing nano-sized reinforcements and/or nano-sized matrix grains. These MMNC materials have recently received a tremendous attention in the hopes of not only attaining superior

Address correspondence to E-mail: kimcs@uwm.edu

DOI 10.1007/s10853-017-1378-x

strength, but also achieving higher ductility than have been obtained with micron-sized reinforcements. In the lightweight structural materials field, Al and its alloys are the most popular base metals in MMC/MMNC that can be widely used for high-performance applications including automotive, military, aerospace, and electricity industries. Al-based composites often exhibit improved physical and mechanical properties such as superior strength to weight ratio, good ductility, high strength and high modulus, low coefficients of thermal expansion (CTE), high wear resistance, and excellent corrosion resistance [4–9].

MMC/MMNC can be manufactured by several synthesis techniques including casting (i.e., solidification) and powder metallurgy (PM) [10–13]. These synthesis techniques can be generally divided into three categories depending on their processing states, (i) liquid-state processing that involves casting, liquid and pressure infiltration, dispersion methods, etc., (ii) solid-state processing which includes PM techniques with variations in the processing steps such as diffusion bonding, sinter forging, etc., and (iii) liquid–solid processing such as compo-casting and semi-solid forming. The details of these processing methods can be found elsewhere [14–16]. Generally, casting is the preferred synthesis method for bulk production with relatively inexpensive processing costs, while PM could be applied to easily control the matrix grain sizes of final products. One of the important advantages of PM is on its low processing temperature compared with the melting techniques, which may reduce the degree of undesired interactions between the Al matrix and reinforcement phases.

Increased strength in these ceramic particulate-reinforced MMCs/MMNCs could be achieved through activation of several strengthening mechanisms such as (i) load transfer [17, 18], (ii) Hall–Petch (i.e., grain refinement) [19, 20], (iii) Orowan [21, 22], (iv) coefficients of thermal expansion (CTE), and/or elastic modulus (EM) mismatch strengthening [23, 24]. Of these, the load transfer and the CTE/EM mismatch strengthening mechanisms can account for the strength increase in the MMC materials with micron-sized particulates, whereas the Orowan effect is supposed to describe the strength increase of MMNC with nano-sized reinforcements, respectively [17, 22, 25]. The Hall–Petch mechanism is one of the primary routes to enhance the strength of both MMC/MMNC systems [19, 24]. The resultant strength increase stems from complicated factors including processing methods/conditions, types of constituent materials, and subsequent microstructural features. Although a certain degree of strength improvement can be achieved in MMC/MMNC by activating some of the preceding strengthening mechanisms, a substantial decrease in energy absorbing abilities (e.g., ductility, toughness, or strain to failure) is commonly observed in these materials [26–28]. One of the contemporary goals of developing advanced MMNC is to minimize such reduction in the ductility of composites.

In the present work, we have comprehensively collected existing data for pure and alloyed Al MMC/MMNC to address various mechanical performances such as (i) yield strength (σ_y), (ii) ultimate strength (σ_{us}), and (iii) strain to failure (ε_f) of the composites. Using the data sets currently available, we attempted to quantitatively analyze the impacts of the microstructural features of composites, (i) reinforcement volume fractions, (ii) reinforcement sizes, and (iii) matrix grain sizes on σ_y, σ_{us}, and ε_f for pure and alloyed Al MMC/MMNC. In addition to the analysis of the microstructure–mechanical property relationship, we attempted to compare the mechanical performance between Al MMC and MMNC and to discuss the strengthening mechanisms. For alloyed Al systems, the trends of collective data sets were considered to examine the general mechanical property changes. In the following section, the features of particulate reinforcements are addressed. The next sections will then include the detailed microstructural and mechanical property information for pure and alloyed Al composites.

Features of particulate reinforcements

In Table 1, some important material properties of ceramic reinforcements commonly used in Al MMC/MMNC are summarized [22, 29, 30]. The thermophysical properties listed here are based on the measurements at room temperature. The CTE values for these materials were approximately linear over the experimental temperature range [31]. Because oxide ceramics are in general very susceptible to plastic deformation at elevated temperatures, they are not considered as structural materials at high-temperature applications [32]. A critical step in the processing of cast particulate-reinforced

Table 1 Typical material properties of ceramic reinforcements [22, 29, 30]

Reinforcements	E (GPa)	K_{IC} (MPa $m^{1/2}$)	UTS (MPa)	CTE, α (10^{-6} K^{-1})	Density, ρ (g cm^{-3})	Poisson's ratio, ν
SiC	450	4.0	310	4.3	3.21	0.17
Al_2O_3	390	4.0	260–300	8.1	3.96	0.25
B_4C	308	2.5	261	5.0	3.25	0.25

E, K_{IC}, *UTS*, and *CTE* denote elastic modulus, fracture toughness, ultimate tensile strength, and the coefficients of thermal expansion, respectively

Table 2 Typical microstructural specifications for Al MMC and MMNC systems

Composite type	Particulate size range of reinforcements (μm)	Volume fraction range of reinforcements (%)	Grain size range of the Al matrix (μm)
MMC	<500	<60	<50
MMNC	<0.1	<10	<50

MMC/MMNC is the incorporation of hard ceramic particulates into the molten Al matrix. In a foundry fabrication method (i.e., casting), controlling the wettability of reinforcement particles is one of the major issues. In general, the ceramic particulates exhibit poor wettability to molten Al metals [33]; the contact angles of Al–Al_2O_3 and Al–SiC were calculated as 97° and 79° at 700 °C, respectively, and the contact angles were found to decrease with increasing temperature [34]. The CTE mismatch between reinforcements and Al matrix is also an essential consideration for composites that will be exposed to thermal cycling [35]. The choice of reinforcement types could be dictated by several factors including particle shapes, processing methods, processing costs, and any desired applications, etc. With these considerations in mind, two reinforcement compounds, SiC and Al_2O_3, have received the most attention in Al MMC/MMNC applications with their relative high modulus and high fracture toughness [36, 37].

Table 2 shows the typical ranges of the reinforcement sizes, volume fractions of reinforcements, and metal-matrix grain sizes that are often observed in Al MMC/MMNC. In the current work, we categorized Al MMNC as the samples with embedded particulate size of less than ~100 nm. Depending on the processing methods, different factors must be taken into consideration to produce high-quality composites. For example, with PM processing, the compositions of the matrix and the types of reinforcements might be controlled in a relatively independent way; however, in casting, they are intimately linked through the reactivity between reinforcements and matrix in the molten state. The distribution of reinforcement particulates is also a critical factor to determine the mechanical properties, and it is greatly influenced by the processing methods. Several advanced synthesis techniques such as stir mixing and ultrasonic mixing can be applied for the homogeneous distribution of particulates in casting. In the PM techniques, some secondary fabrication methods such as extrusion and rolling are essential in the composite processing, and these post-processing methods have been identified to improve the physical properties of composites by redistributing the reinforcement arrangements [38]. In PM-processed composite materials, the distribution aspects of reinforcement particles will depend on the blending and the consolidation procedures as well as the matrix-to-reinforcement particle size ratios (PSR). If the size of matrix powders is large relative to the size of reinforcements, the reinforcing particles tend to segregate in the interstices of the coarse-grained matrices. In composites processed by molten metal mixing methods (i.e., casting), the particulate distribution features could be more complicated because the distribution is influenced by numerous processing factors such as the particle distribution in the liquid and the particle redistribution as a result of solidification.

Pure Al systems

In Tables 3 and 4, we summarized the currently available data for the reinforcement types, processing methods/conditions, reinforcement fractions/sizes,

matrix grain sizes, and resultant mechanical properties including the yield strength (σ_y), ultimate strength (σ_{us}), and strain to failure (ε_f) for pure Al MMC (Table 3) and MMNC (Table 4) systems, respectively [14, 39–50]. Instead of ultimate tensile or compressive strength (i.e., σ_{uts} or σ_{ucs}, respectively), σ_{us} was used because some of the existing ultimate strength data are based on the compression tests. In the tables throughout this document, (C) indicates the properties obtained through the compression tests. In the following subsections, we address the effects of the reinforcement volume fractions, reinforcement sizes, and matrix grain sizes on σ_y, σ_{us}, and ε_f of pure Al-based composites. Note that although similar processing techniques (e.g., PM + extrusion) may have been applied to produce some of the collected examples shown in Tables 3 and 4, experimental conditions such as the sizes of starting powder/particle, extrusion temperatures, and extrusion ratios are vastly different.

Particle volume fraction effects

MMCs

Figure 1 shows the selected examples of (a) σ_y, (b) σ_{us}, and (c) ε_f variations along with the particulate volume fractions for pure Al MMC systems listed in Table 3. In general, as the volume fraction of reinforcements increases, σ_y and σ_{us} initially increase and then decrease, and ε_f decreases, respectively. The decrease in σ_y and σ_{us} with high reinforcement vol% is generally observed in both MMC and MMNC and is commonly explained by the clustering of reinforcements and by the formation of weak regions in the composites [41]. Homogeneous and uniform distribution of reinforcement particles depends not only on the particle contents but also on the matrix-to-reinforcement PSR. Although a homogeneous distribution of embedded particulates is highly desired, it can be hardly achieved when the PSR value is large [51]. Due to the decay of these σ_y and σ_{us} beyond a certain amount of reinforcement addition, identification of the peak particulate vol% position to produce maximum σ_y and/or σ_{us} is one of the primary concerns in designing MMCs/MMNCs. The peak positions of reinforcement vol% to exhibit the best performance could be largely different. One of the reasons for such difference in the peak positions is correlated with the reinforcement particle size; there would be a high propensity for clustering when the particulate size is smaller, and this clustering of particles will decrease the strength of composites at a lower reinforcement vol%. This trend is clearly shown in Fig. 1a, b; as the particulate sizes increase from 0.47 [43] → 3–48 [42] → 70 [14] μm, the peak vol% values for σ_y and σ_{us} shift from 2% → 7% → none. In Al/SiC composites in Ref. [14], the decrease in σ_y and σ_{us} was not even observed, which implies that considerable clustering/segregation of reinforcement particulates did not occur in the composite structure up to 20 vol% of particulate addition. In the Al/Al_2O_3 composites [42] shown in Fig. 1b, there is a maximum σ_{us} for the samples with particle sizes of 3 and 12 μm, while no prominent maximum is observed for the sample reinforced by 48 μm particle size. This indicates a lower tendency for clustering in the composites with larger particles, which could be attributed to a higher specific surface area of smaller particles. Also, the difference in the peak vol% position could be resulted from different processing methods. If a high degree of porosity is generated during synthesis, the peak vol% position may be significantly lowered.

Note that σ_y and σ_{us} of the monolithic pure Al (i.e., non-reinforced samples, 0% reinforcement fractions) show different strength values in Fig. 1a, b. As there is no alloying effect in the matrix for these pure Al matrix samples, such initial differences in σ_y and σ_{us} presumably come from the differences in their metal-matrix grain sizes and the initial dislocation densities derived from various processing methods and heat treatment histories. However, in many of the previous experiments, measurements for the matrix grain size have not been quantitatively performed. For example, in Refs. [14, 41, 43], information for the initial Al powder sizes is sometimes provided, but the grain sizes of monolithic unreinforced Al samples were not provided. The samples reinforced by SiC particles [14] showed relatively low strength even at the particulate vol% of 20. The reason is explained by the grain coarsening resulted from hot extrusion; the sintered specimens (at 575 °C for 10 h) were hot extruded to rods at 570 °C with an extrusion ratio of 9:1 to form tensile test samples. The difference in σ_{us} of Al/SiC [14] and Al/Al_2O_3 [42] composites can be related to many factors such as the dissimilar particulate types (SiC and Al_2O_3), particulate sizes (70 and 3–48 μm), testing types (tensile and compression

Table 3 Reinforcement types, processing methods, microstructural features, and mechanical properties of pure Al MMC systems

Reinforcement types (references)	Processing methods/conditions	Reinforcement		Grain size, D (μm)	Mechanical properties			
		Volume fraction (vol%)	Particle size (μm)		E (GPa)	σ_y (MPa)	σ_{us} (MPa)	ε_f (%)
SiC [14]	PM + extrusion (570 °C)	0	70 (Avg)	40 (Avg)		56.6	84	26.2
		4				58.3	91	14.1
		8				59.7	96	12.5
		12				61.4	103	9.5
		16				62.9	115	8.4
		20				64.6	127	7.2
SiC [39]	PM + extrusion	0	13	4.6		75	150	20
		10		–		110	185	18
SiC [40]	PM + extrusion (430 °C)	20	4.7			87.5	120	3.9
			16.7			86	105	4.1
			39.1			85.5	102	5.1
			70.7			85	95	5.3
Al_2O_3 [41]	PM	10 (wt%)	3	30 (Avg)		205 (C)	275 (C)	47 (C)
	500 °C		12			177 (C)	248 (C)	28 (C)
			48			138 (C)	151 (C)	16 (C)
	PM		3			224 (C)	306 (C)	58 (C)
	550 °C		12			188 (C)	273 (C)	35 (C)
			48			161 (C)	167 (C)	19 (C)
	PM		3			238 (C)	317 (C)	63 (C)
	600 °C		12			210 (C)	294 (C)	50 (C)
			48			187 (C)	205 (C)	33 (C)
Al_2O_3 [42]	PM	0 (wt%)	3	30 (Avg)		114 (C)	130 (C)	60 (C)
		5 (wt%)				157 (C)	224 (C)	58 (C)
		10 (wt%)				224 (C)	310 (C)	55 (C)
		20 (wt%)				193 (C)	238 (C)	40 (C)
		0	12			114 (C)	130 (C)	60 (C)
		5				134 (C)	190 (C)	39 (C)
		10				190 (C)	273 (C)	33(C)
		20				162 (C)	188 (C)	29 (C)
		0	48			114 (C)	130 (C)	60 (C)
		5				120 (C)	136 (C)	25 (C)
		10				159 (C)	165 (C)	19 (C)
		20				137 (C)	144 (C)	15 (C)
Al_2O_3 [43]	Accumulative roll bonding (ARB)	0	0.47			160	186	12.1
		1				193	221	8.5
		2				215	279	7.6
		3				210	257	4.0

Table 3 continued

Reinforcement types (references)	Processing methods/conditions	Reinforcement		Grain size, D (μm)	Mechanical properties			
		Volume fraction (vol%)	Particle size (μm)		E (GPa)	σ_y (MPa)	σ_{us} (MPa)	ε_f (%)
Al_2O_3-SiC [44]	Annealing + Accumulative roll bonding (ARB)	0	50–75			45	87	30
		1.6–0.5				223	260	13
		1.6–1				260	284	11
		1.6–2				250	269	8

(C) indicates the results from compression test

tests), and processing methods (with and without extrusion).

As shown in Fig. 1c, the variations of ε_f with particle vol% clearly present the consistent impacts of reinforcement vol% on the ductility of Al MMCs; ε_f decreases as the reinforcement vol% increases. The reduction of ε_f in the samples with higher vol% of reinforcement particulates is explained by substantially lower ε_f of brittle ceramic particles and by a higher degree of particle agglomeration/clustering. Figure 1c also shows the effects of Al_2O_3 sizes on ε_f [42]; as the size of the Al_2O_3 reinforcement particles increases, the measured ε_f value decreases. This decrease is even greater in the specimens with the particle sizes ranging from 12 to 48 μm due to a smaller density and a larger porosity in these specimens. Larger porosity could be originated from the decline in the pressing capability of samples with larger contents of Al_2O_3. Prohibitive effects of Al_2O_3 particulates on sintering mechanisms might be another reason for this phenomenon. Due to its high melting point, Al_2O_3 will be likely to form a weak bonding to pure Al, which can lead to a weaker network.

MMNCs

Analogous to the MMC case, it is generally expected that the strength (σ_y and σ_{us}) and the ductility (or strain to failure, ε_f) of MMNC are increased and then decreased and decreased, respectively, with increasing the vol% of reinforcement particulates. Figure 2a–c provides the plots of selected data sets from Table 4 to display (a) σ_y, (b) σ_{us}, and (c) ε_f variations with reinforcement vol% in pure Al MMNC systems. Compared with MMC materials, the reinforcement vol% incorporated in MMNC systems is typically much smaller, because of a much stronger propensity for agglomeration of nano-sized reinforcements during synthesis. From Fig. 2a, one can clearly see that Al/Al_2O_3 MMNC shows a wide range of σ_y with various reinforcement vol% in the composites [39, 45, 48, 50]. As mentioned earlier, the reinforcement vol% is not the only parameter determining mechanical properties. One of the reasons for the difference in σ_y shown in Fig. 2a is accounted for the sample fabrication history. Kang and Chan [39] employed the following sequential steps to prepare their tensile test samples: (i) cold isostatic processing (CIP) at 150 °C, (ii) sintering at 620 °C for 2 h, (iii)

Table 4 Reinforcement types, processing methods, microstructural features, and mechanical properties of pure Al MMNC systems

Reinforcement types (references)	Processing methods/conditions	Reinforcement		Grain size, D (μm)	Mechanical properties			
		Volume fraction (vol%)	Particle size (nm)		E (GPa)	σ_y (MPa)	σ_{us} (MPa)	ε_f (%)
SiC [45]	MA + consolidation	0	50	0.7		164 (C)	302 (C)	22.5 (C)
		1		0.35		207 (C)	385 (C)	18 (C)
		3		0.23		219 (C)	426 (C)	15.5 (C)
		5		0.17		258 (C)	436 (C)	7.5 (C)
		7		0.15		269 (C)	448 (C)	5.5 (C)
SiC [46]	Planetary milling	0	~50				–	–
		1					205	17
		5					–	–
		10					405	4
		20					–	–
Al_2O_3 [47]	Ultrasonic casting	0	10	40–75	69.3 ± 1.7	30	62	47
		1.4			76.4 ± 2.2	47	91.6	36
Al_2O_3 [39]	PM + extrusion	0	50	4.6		75	150	27
		1		3.0		115	180	21
		2		2.3		125	210	18
		3		1.9		155	230	15
		4		1.2		180	245	13
		5		1.1		175	235	9
		6		1.2		170	250	10
		7		1.3		185	245	8
Al_2O_3 [48]	PM	0 (wt%)	35			80	120	
		2 (wt%)				120	215	
		3 (wt%)				145	250	
		4 (wt%)				170	280	
		5 (wt%)				150	255	
		6 (wt%)				140	230	
B_4C [49]	Ball milling (BM) + hot press	0 (wt%)	10–60	0.08	–	–	–	–
		5 (wt%)			47.5	324 (C)	371 (C)	16.3 (C)
		10 (wt%)			52.5	385 (C)	433 (C)	14.1 (C)
		15 (wt%)			54	420 (C)	485 (C)	12.1 (C)
Al_2O_3–B_4C [50]	MA	0	50	0.54		129	161	
		1		0.44		193	228	
		2		0.4		215	246	
		4		0.23		241	279	

extrusion at 420 °C with a ratio of 36:1, and (iv) annealing at 350 °C for 2 h. On the other hand, the sample preparation procedure used in Ref. [48] is: (i) ball milling (BM), (ii) compaction at 140 MPa, and (iii) hot extrusion at 600 °C with a ratio of 20:1. Alizadeh [50] roll-bonded the billets at room temperature with a 50% ratio for 9 cycles. From these, it is appreciable that higher plastic deformation prior to the tensile testing can produce a sample with finer grains along with higher σ_y and σ_{us} (i.e., work-hardening effect). In Fig. 2a, different peak positions for σ_y are observed in Refs. [39] and [48], where Al/Al_2O_3 MMNC was prepared using PM processes. Powder compaction step was followed by sintering at 620 °C for 2 h in Ref. [39], while a hot forward extrusion process at 600 °C was employed instead of sintering to obtain a highly dense product in Ref. [48]. As previously discussed, a lower porosity in the synthesized sample can be obtained at an elevated sintering temperature, and a higher degree of

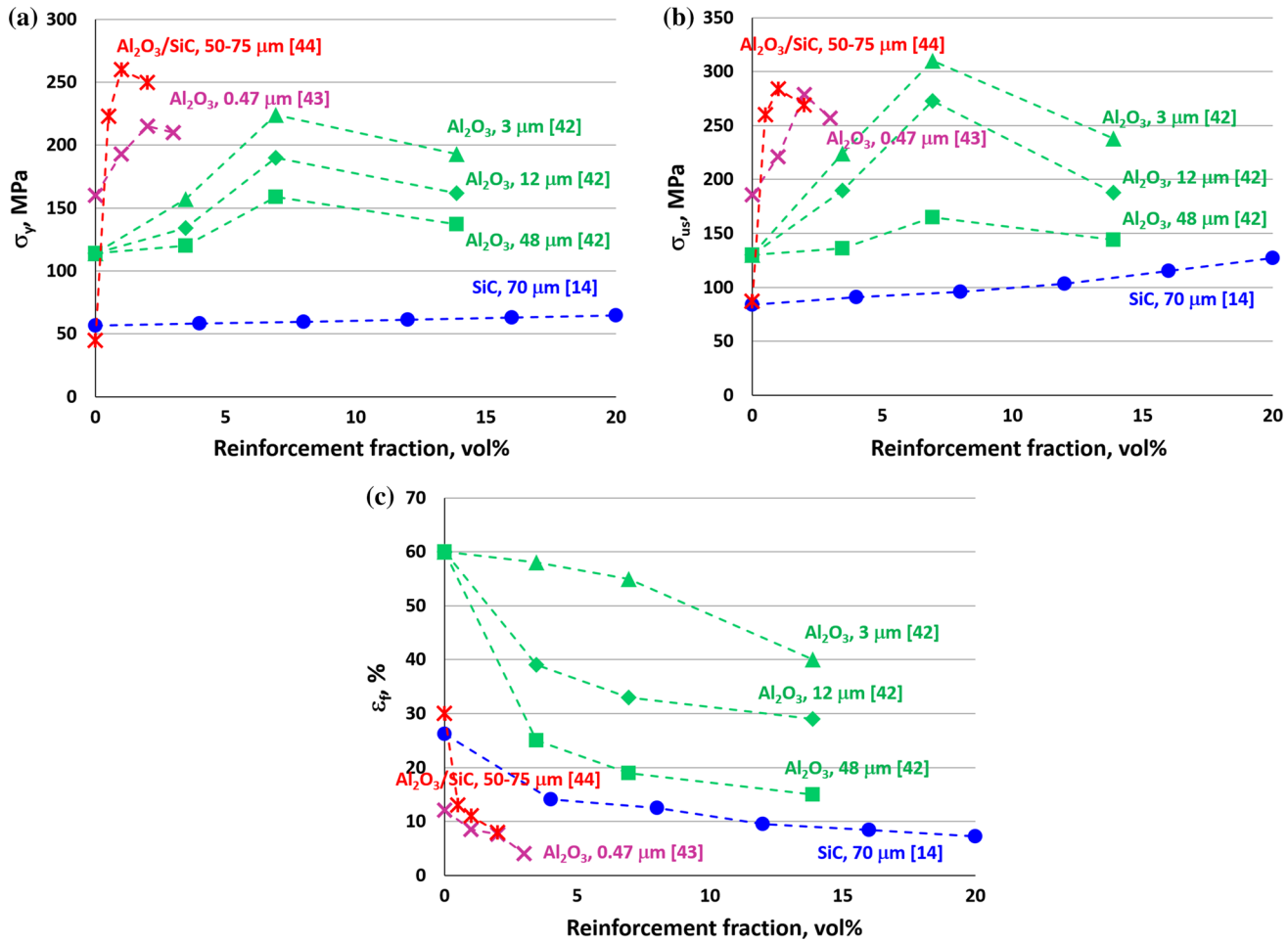

Figure 1 Effects of particle volume fractions on **a** σ_y, **b** σ_{us}, and **c** ε_f for pure Al MMC systems.

porosity may cause a significantly lower peak position [41]. It is notable that, sometimes, the increasing and decreasing trend for σ_y with reinforcement vol% is not found in the experiments as exemplified in Refs. [45, 50]. Alizadeh [50] employed Al_2O_3/B_4C nanoparticles as the reinforcement materials, and no local maximum σ_y was monitored in the produced composite up to 4 vol% of Al_2O_3/B_4C. In his work, microstructural characterization revealed a fairly uniform distribution of the nano-sized Al_2O_3/B_4C particles. The author claimed that increased number of Al and Al_2O_3/B_4C layers, the metal extrusion through particle clusters, and the sheet elongation due to rolling, are the main reasons to observe uniform distribution of the Al_2O_3/B_4C reinforcements. No σ_y peak position was observed in Ref. [45] as well, as the SiC clusters and the SiC-free regions were found to decrease with increasing the SiC contents. However, it is not currently certain that how much reinforcement vol% could be added to these samples without σ_y peak positions beyond 4 vol%.

In Fig. 2b, the σ_{us} variations in Al MMNCs with reinforcement vol% are presented. As explained before, minimal degrees of particle clustering are reported in the samples of Refs. [45] and [50]; therefore, σ_{us} in these examples continuously increases as the reinforcement vol% increases. When the results for the effects of the reinforcement vol% on σ_y and σ_{us} are compared, the optimum vol% values of the reinforcement contents to show the best performance are nearly identical for σ_y and σ_{us}. This is generally true for the cases of both MMC and MMNC. These optimal reinforcement vol% values are determined by many factors including material types and processing histories. It is once more generally expected that, with increasing reinforcement contents, ε_f of

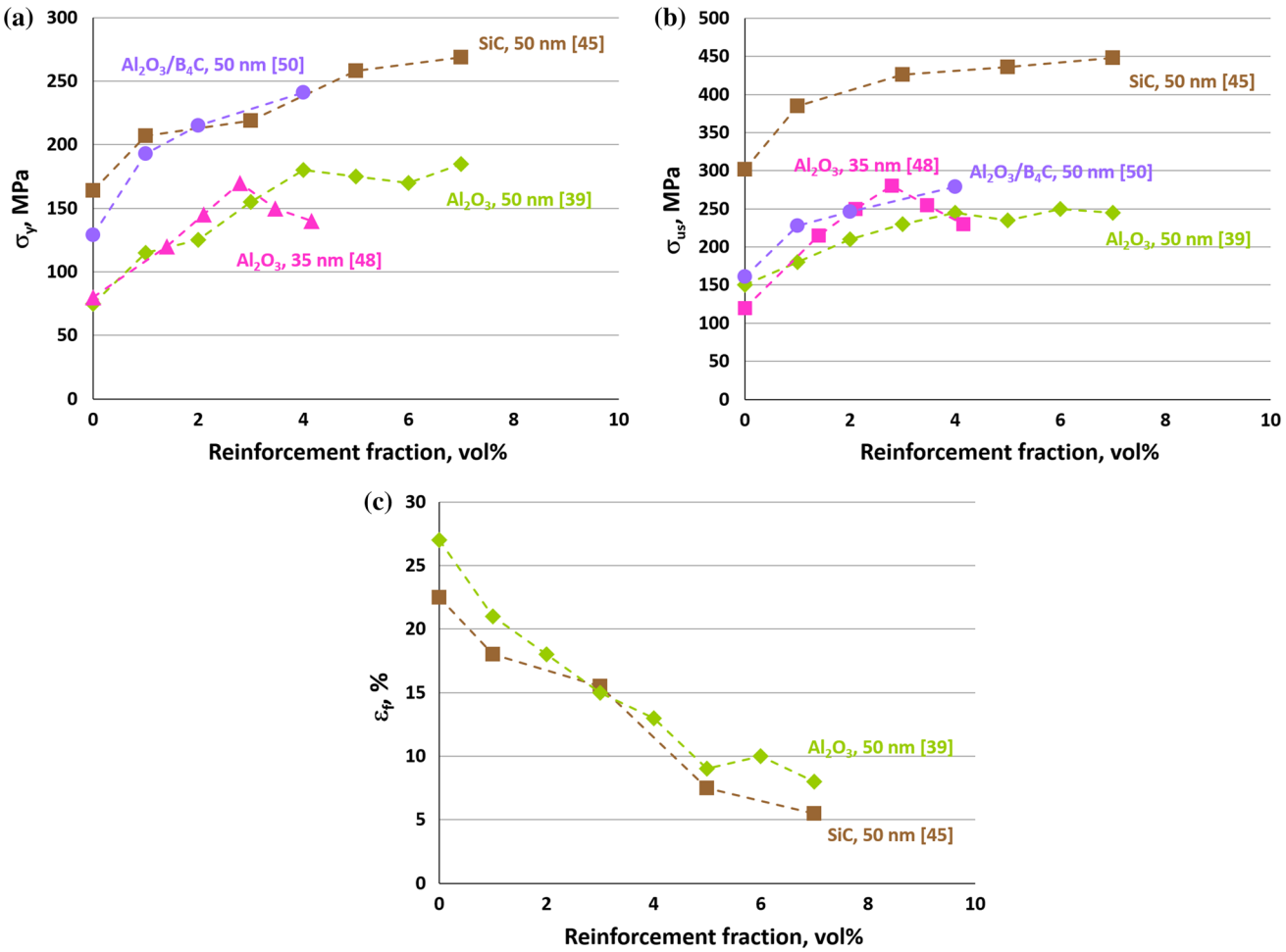

Figure 2 Effects of particle volume fractions on **a** σ_y, **b** σ_{us}, and **c** ε_f for pure Al MMNC systems.

MMNC decreases because the distance between the hard phases decreases with a higher amount of reinforcements, which hinders the dislocation movements. Note that ε_f measurement values are not reported for Al MMNC in many literature most likely because Al MMNC composites containing nano-sized reinforcement particles often show very poor ductility. Figure 2c shows two selected examples of the ε_f variations with the reinforcement vol% in Al MMNC. Different starting points and decreasing rates of ε_f were observed in the ε_f vs. reinforcement vol% plots that may be resulted from different material types, microstructures, and processing conditions.

Particle size effects

It is identified that the reinforcement sizes can impose an indirect effect on the mechanical properties of the Al MMC, an increasing trend in σ_y and σ_{us} with decreasing particle sizes. This trend is clearly reported in Ref. [42], as shown in Fig. 1a, b. Here, when the Al_2O_3 reinforcement particulate size increases from 3 to 48 μm, measured σ_y and σ_{us} were substantially decreased in the entire reinforcement vol% ranges. This can be explained by the dispersion strengthening mechanism in Al matrix [52]; decreasing the particulate size in a certain volume fraction leads to a decrease in the distance between the particulates, which increases the required tension for dislocation movements between the reinforcement particulates, thereby increasing the strength of composites. Also, smaller particles will indirectly increase the strength by slowing down the grain growth during processing (i.e., grain refinement mechanism). An increasing trend in ε_f with decreasing particle size is expected for Al MMCs as presented in Fig. 1c [41, 42]; however, there would be an optimal minimum size of reinforcements because smaller

particulates show much higher tendency for agglomeration upon synthesis, which will substantially deteriorate the strength and the ductility of composites. Therefore, the optimal particulate size must be carefully determined considering the material types and synthesis conditions. As for the impacts of particulate size on the mechanical performance of pure Al MMNCs, not sufficient data are currently available partly because the variation of nano-sized particulate sizes is rather limited and a uniform size of particulates is routinely added into the Al matrix.

Matrix grain size effects

The matrix grain size of Al MMC/MMNC is also a vital factor to determine various mechanical properties of composites. The grain sizes of synthesized composites are highly influenced by the amounts of added reinforcement particles [39, 45, 50]. It is generally understood that as greater reinforcement contents are added with smaller particles, more refined grain structures are obtained [53]. This is because the particulates can pin the grain boundaries and prevent the grain growth of Al matrix during synthesis. Such grain boundary pinning effects are observed nearly all Al MMC/MMNC including Al_2O_3, B_4C, and SiC particulates. In Ref. [41], it was observed that any increase in reinforcement particulate contents leads to finer grain sizes in pure Al MMC samples containing 5–20 wt% Al_2O_3. Kang and Chan [39] showed that the grain sizes of Al/Al_2O_3 composites decreased when the embedded reinforcement contents increased from 0 to 4 vol% and remained unchanged for further addition of reinforcements. It also has been found that the B_4C nanoparticles can lock the Al grain boundaries and prevent a significant grain growth during hot pressing [49] and that SiC particles can retard the grain growth during sintering producing ultrafine grain structures [45]. Although it is known that the reinforcement contents largely affect the matrix grain size, there could be a wide range of differences in the quantitative impacts of reinforcement particulate on the final grain size, and the observed difference is generally associated with the reinforcement particulate sizes/amounts, starting monolithic matrix grain sizes, and fabrication conditions.

Strengthening mechanisms

In Fig. 3a, we present selected examples of the comparison between experimental (measured) and theoretical (calculated) σ_y values for pure Al MMNC samples listed in Table 4. Theoretical σ_y of particulate-reinforced MMNC materials can be estimated by the following considerations [54, 55].

$$\text{Arithmetic summation: } \sigma_y = \sigma_0 + \Delta\sigma_{HP} + \Delta\sigma_{OR} + \Delta\sigma_{CTE} + \Delta\sigma_l \quad (1)$$

$$\text{Quadratic summation: } \sigma_y = \sigma_0 + \sqrt{\Delta\sigma_{HP}^2 + \Delta\sigma_{OR}^2 + \Delta\sigma_{CTE}^2 + \Delta\sigma_l^2} \quad (2)$$

$$\Delta\sigma_{HP} = k_y\left(\frac{1}{\sqrt{d_{MMNC}}} - \frac{1}{\sqrt{d_0}}\right) \quad (3)$$

$$\Delta\sigma_{OR} = \frac{0.13G_m b}{\lambda}\ln\left(\frac{d_p}{2b}\right) \quad (4)$$

$$\Delta\sigma_{CTE} = \sqrt{3}\beta G_m b\sqrt{\rho_{CTE}} \quad (5)$$

$$\Delta\sigma_l = \frac{1}{2}V_p\sigma_0 \quad (6)$$

where σ_0 is the original yield strength of the monolithic metal matrix, and $\Delta\sigma_{HP}$, $\Delta\sigma_{OR}$, $\Delta\sigma_{CTE}$, and $\Delta\sigma_l$ are the yield strength increases from the CTE mismatch between the reinforcements and metal matrix, Orowan strengthening, Hall–Petch strengthening, and load-bearing strengthening contributions, respectively. To theoretically evaluate the individual contributions from different strengthening mechanisms, material and processing variables including k_y (Hall–Petch constant), G_m (shear modulus), b (Burgers' vector), β (dislocation strengthening coefficient), and α (CTE values) need to be quantified. In Eqs. (3)–(6), d_{MMNC}, d_0, d_p, V_p, $\lambda = d_p\left(\frac{1}{(2V_p)^{1/3}} - 1\right)$, and $\rho_{CTE} = \frac{12V_p\Delta\alpha\Delta T}{(1-V_p)bd_p}$, respectively, stand for the average grain size of MMNC composites, average grain size of monolithic Al, particulate diameter, particulate volume, interparticle mean free path, and dislocation density created by the CTE strengthening. As introduced in Eqs. (1) and (2), the arithmetic and quadratic summation methods can be independently applied in the theoretical estimation of σ_y, but it was claimed that the quadratic summation method produces more reasonable results compared with the arithmetic summation method [55]. In the current study, for the theoretical increase of σ_y shown in

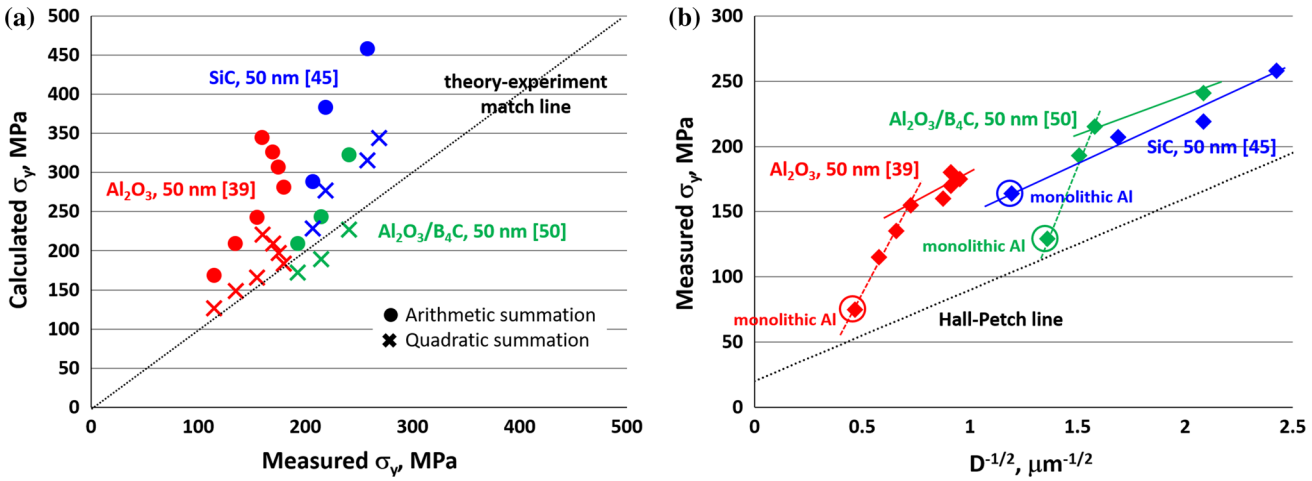

Figure 3 **a** Comparison between experimental (measured) and theoretical (calculated) σ_y values and **b** variations of experimental σ_y with the inverse of square root of matrix grain sizes ($D^{-1/2}$) for pure Al MMNC systems.

Table 5 Parameters used for the σ_y estimation of pure Al MMNC systems [38, 50]

Strengthening mechanism	Parameter		Value
Hall–Petch ($\Delta\sigma_{HP}$)	Yield strength of monolithic Al, σ_0 (MPa)		20.0
	Hall–Petch constant, k_y (MPa $\mu m^{0.5}$)		70.0
Orowan ($\Delta\sigma_{OR}$)	Shear modulus, G_m (GPa)		26.0
	Burgers' vector, b (nm)		0.286
	Poisson's ratio, v		0.345
CTE mismatch ($\Delta\sigma_{CTE}$)	Dislocation strengthening coefficient, β		0.424
	CTE, α ($\times 10^{-6}$ K^{-1})	α_{Al}	24.0
		$\alpha_{Al_2O_3}$	7.4
		α_{B_4C}	5.0
		α_{SiC}	4.0

Fig. 3a, the material parameters listed in Table 5 are used [38, 50]. The CTE was assumed as a constant for Al, Al_2O_3, B_4C, and SiC; although the CTE values of these materials will vary with temperature changes, it was expected that the error originated from this constant CTE assumption would be as large as ~2% [54]. In Fig. 3a, theoretically calculated σ_y results for pure Al MMNC using the arithmetic and the quadratic summation approaches are given by the circular and cross-marked symbols, respectively. Results from Refs. [39, 45, 50] are reported here because these are the only resources to report all necessary microstructural parameters including matrix grain sizes. The diagonal line in Fig. 3a represents the one-to-one correspondence between calculated and measured σ_y. If individual contributions from different strengthening mechanisms are examined, the contributions from $\Delta\sigma_{HP}$, $\Delta\sigma_{OR}$, and $\Delta\sigma_{CTE}$ are largely dominant and that of $\Delta\sigma_l$ is relatively minor. When theoretically estimated σ_y is compared with experimentally measured σ_y, one can readily notice that the σ_y values based on the quadratic summation are generally much closer to the experimental measurements. In addition, in many cases, the theoretical calculation overestimates σ_y, which indicates that the individual strengthening mechanisms addressed in Eqs. (1) and (2) are not fully activated in these Al MMNC systems.

To further examine the strengthening mechanisms in pure Al MMNC systems, in Fig. 3b, we plotted the

Table 6 Reinforcement types, processing methods, microstructural features, and mechanical properties of Al alloy MMC systems

Reinforcement types [Ref]	Alloy types	Processing methods/conditions	Reinforcement		Grain size, D (μm)	Mechanical properties			
			Volume fraction (vol%)	Particle size (μm)		E (GPa)	σ_y (MPa)	σ_{us} (MPa)	ε_f (%)
SiC [56]	2014 AA	As cast	0 (wt%)	40–65		73 (C)	180 (C)	375 (C)	23 (C)
			5 (wt%)			84 (C)	210 (C)	400 (C)	15 (C)
			10 (wt%)			94 (C)	225 (C)	430 (C)	14 (C)
		Heat-treated				75 (C)	384 (C)	580 (C)	22 (C)
						86 (C)	300 (C)	485 (C)	17 (C)
						93 (C)	360 (C)	585 (C)	18 (C)
SiC [57]	Al-Cu alloy	BM for 2 h	20	4.7	60		158	215	1.80
		BM for 7 h					175	230	2.10
		BM for 16 h					150	190	1.40
		BM for 40 h					200	250	2.30
				77			125	155	2.50
							160	190	2.90
							165	200	3.00
							180	210	3.20
SiC [58]	Al-Cu alloy	BM for 7 h	0	77	60		62	70	
			10				70	80	
			15				78	85	
			20				96	100	
		BM for 7 h extruded-aged for 8 h					200	300	
							160	195	
							150	185	
							120	175	
		BM for 7 h extruded-aged for 20 h					225	330	
							185	225	
							180	220	
							145	195	
		BM for 7 h extruded-aged for 24 h					185	280	
							165	215	
							160	210	
							120	165	
SiC [59]	2080 AA	Experiment	0			73			
			10			88			
			20			109			
			30			125			

Table 6 continued

Reinforcement types [Ref]	Alloy types	Processing methods/conditions	Reinforcement		Grain size, D (μm)	Mechanical properties			
			Volume fraction (vol%)	Particle size (μm)		E (GPa)	σ_y (MPa)	σ_{us} (MPa)	ε_f (%)
SiC [60]	6061 AA	0% rolled	10				35	65	2.4
		30% rolled					–	90	2.8
		60% rolled					80	125	3.4
		75% rolled					–	190	4.2
		85% rolled					120	245	6.2
		95% rolled					155	305	8.0
SiC [61]	1050 AA	ABR (11 cycles)	10	2				220	6
				40				205	8
SiC [62]	Al–Mg–Cu alloy	Squeeze casting	0	36			183	247	3.30
			5				187	216	1.53
			10				224	232	0.70
			15				–	239	0.45
SiC [63]	Al–Cu alloy	PM + solution heat-treated	0	3	40	76	151	327	35.8
			5			83	200	392	21.8
			10			91	241	409	10.8
			15			92	264	391	5.7
			20			91	277	366	2.7
		PM + aged				76	297	414	17.9
						83	326	456	12.0
						91	360	474	6.6
						92	359	446	2.6
						91	327	386	0.7
		PM + solution heat-treated	5	14	40	89	199	376	22.2
			10			93	231	388	16.6
			15			93	256	398	10.7
			20			110	266	378	6.7
		PM + aged				89	310	440	13.0
						93	341	458	9.0
						93	366	468	4.7
						110	385	468	2.7
		PM + solution heat-treated	15	14	80	92	145	236	9.4
		PM + aged				92	375	447	2.6
		PM + solution heat-treated			130	90	146	219	7.1
		PM + aged				90	360	423	2.4
		PM + solution heat-treated			180	85	134	192	4.6
		PM + aged				85	335	371	1.0

Table 6 continued

Reinforcement types [Ref]	Alloy types	Processing methods/conditions	Reinforcement		Grain size, D (μm)	Mechanical properties			
			Volume fraction (vol%)	Particle size (μm)		E (GPa)	σ_y (MPa)	σ_{us} (MPa)	ε_f (%)
SiC [64]	7075 AA	Co-sprayed deposition (CSD, under aged)	15	5			499	609	10.4
				13			502	595	6.8
				60			431	453	1.2
		CSD, peak aged					570	630	6.6
							595	645	3.5
							501	504	0.6
		CSD, over aged					510	574	6.3
							539	596	3.9
							484	493	0.8
SiC [65]	2024 AA	Powder centrifugal atomization + hot extrusion	0	125			75	185	21.0
			3				175	264	5.1
			5				214	320	3.2
			7				221	374	7.0
			10				210	308	6.6
SiC [66]	356 AA	Vortex method	0	16				68	
			10					88	
			20					100	
			30					112	
SiC [67]	Al–Cu alloy	Hot press	0	10	25	70	110	206	21.5
			15			82.560	142	212	7.6
			30			93.100	174	241	1.8
					100		118	213	17.2
							140	212	5.9
							130	246	2.6
SiC-mica [68]	356 AA	Stir casting	0 (wt%)					146	
			3 (wt%)					150	
			6 (wt%)					148	
SiC-RHA (rice husk ash) [69]	356 AA	Double stir casting	0 (wt%)				168	263	7.35
			2 (wt%)				182	296	6.25
			4 (wt%)				196	310	5.6
			6 (wt%)				230	333	5.15
			8 (wt%)				258	356	4.9

Table 6 continued

Reinforcement types [Ref]	Alloy types	Processing methods/conditions	Reinforcement		Grain size, D (μm)	Mechanical properties			
			Volume fraction (vol%)	Particle size (μm)		E (GPa)	σ_y (MPa)	σ_{us} (MPa)	ε_f (%)
Al_2O_3 [70]	356 AA	Stir casting	0	20	–			234 (C)	
			1		52			251 (C)	
			3		58			311 (C)	
			5		55			391 (C)	
			10		71			453 (C)	
Al_2O_3 [71]	356 AA	Casting	0 (wt%)	30			90 (C)	214 (C)	
			1 (wt%)				120 (C)	264 (C)	
Al_2O_3 [72]	356 AA	Stir casting	0 (wt%)				82	133	1.55
			1 (wt%)				87	140	1.45
			3 (wt%)				94	148	0.94
			5 (wt%)				102	155	0.83
			7.5 (wt%)				92	153	0.65
		Compo-casting					82	133	1.55
							87	143	1.48
							95	147	1
							102	156	0.87
							95	149	0.7
Al_2O_3 [73]	2024 AA	Vortex method	0	16				68	
			10					88	
			20					96	
			30					110	
				32				68	
								90	
								98	
								105	
				66				68	
								80	
								83	
								89	

Table 6 continued

Reinforcement types [Ref]	Alloy types	Processing methods/conditions	Reinforcement		Grain size, D (μm)	Mechanical properties			
			Volume fraction (vol%)	Particle size (μm)		E (GPa)	σ_y (MPa)	σ_{us} (MPa)	ε_f (%)
Al_2O_3 [74]	356 AA	Squeeze casting	0	0.3–0.5				397	
			10					482.5	
			20					463.8	
			30					457	
			40					443	
	6061 AA		0	0.3–0.5				397	
			10					463.3	
			20					447.7	
			30					441.2	
			40					435.1	
	1050 AA		0	0.3–0.5				397	
			10					348.8	
			20					418.7	
			30					412.4	
			40					407.2	
Al_2O_3 [75]	6061 AA	Stir casting	0 (wt%)	125				150	15.56
			3 (wt%)					165	12.32
			6 (wt%)					173	10.68
			9 (wt%)					175	8.34
Al_2O_3 [76]		PM + extrusion	0	20		–	106	178	22
			5				100	190	22
			10				99	190	20
			15				102	185	19
			20				110	198	15
			25				112	189	15
			30				120	190	10
		PM				68	295	315	10
						77	335	355	9
						82	325	350	8
						85	325	350	6
						89	305	340	5
						93	320	355	3
						96	320	350	2

Table 6 continued

Reinforcement types [Ref]	Alloy types	Processing methods/conditions	Reinforcement		Grain size, D (μm)	Mechanical properties			
			Volume fraction (vol%)	Particle size (μm)		E (GPa)	σ_y (MPa)	σ_{us} (MPa)	ε_f (%)
Al_2O_3 [77]	6061 AA	PM	0(wt%)			68.03		121.53	29.26
			10(wt%)			86.81		328.22	4.72
			20(wt%)			104.45		410.10	2.29
			30(wt%)			109.9		448.77	1.42
$Al_6Si_2O_{13} + Al_2O_3$ [78]	6061 AA	PM	0	20		68.02	105.70	78.79	21
			5			76.35	99.65	189.84	22
			10			80.73	99.61	189.37	19
			15			84.48	102.64	185.58	18
			20			88.54	110.26	198.05	13
			25			92.60	112.17	190.79	13
			30			95.10	122.18	195.53	9
Al_2O_3 [79]	6061 AA	Stir casting	0 (wt%)	125			138.06	149.76	15
			6 (wt%)				145.51	167.93	13
			9 (wt%)				155.94	173.61	12
			12 (wt%)				178.91	193.47	10.8
Al_2O_3-CNT [80]	356 AA	Infiltration method	0					110 (C)	
			10–2					120 (C)	
			15–2					140 (C)	
			20–2					170 (C)	
Al_2O_3–B_4C [81]	LM25	Stir casting	65		1.71		68.24	4.00	65
					1.37		54.60	4.00	
					1.39		51.75	3.71	
B_4C [82]	1100 AA	Accumulative roll bonding (ARB)	0	3	151		80	120	
			1.1				310	370	
B_4C [83]	7075 AA	Hot press	0	16–20				220	
			5					245	
			10					255	
			15					285	
			20					300	
TiB_2 [84]	7075 AA	Stir casting	0 (wt%)					140	8.2
			3 (wt%)					200	7.9
			6 (wt%)					245	4.9
			9 (wt%)					286	3.3

Table 6 continued

Reinforcement types [Ref]	Alloy types	Processing methods/conditions	Reinforcement		Grain size, D (μm)	Mechanical properties			
			Volume fraction (vol%)	Particle size (μm)		E (GPa)	σ_y (MPa)	σ_{us} (MPa)	ε_f (%)
TiB_2 [85]	6061 AA	Stir casting	0(wt%)					89.54	
			4(wt%)					98.31	
			8(wt%)					113.03	
			12(wt%)					137.86	
TiB_2 [86]	356 AA	Stir casting	0	5		70.73	237	242.6	
			0.5			77.39	223	236	
			1.5			77.67	237	272	
			3			79.71	271	308	
			5			78.29	244	281	

variations of measured σ_y for the Al composites in Fig. 3a with changes of inverse of square root of average matrix grain size ($D^{-1/2}$). The dotted line in Fig. 3b represents the expected σ_y from the Hall–Petch relation using the σ_0 and k_y parameters in Table 5. In the figure, measured σ_y values of monolithic Al materials are indicated using circles, which should be theoretically positioned on the Hall–Petch line. The measured σ_y of monolithic Al (i.e., blue circle in Fig. 3b) for Ref. [45] is much higher than the expected value probably due to the intensive mechanical alloying during synthesis. When the variations of measured σ_y of the MMNC materials are examined for Al_2O_3 composites studied in Refs. [39, 50], the initial slope (indicated as a dashed line) is much greater than that of Hall–Petch line, which obviously elucidates that other strengthening mechanisms in addition to the grain refinement have been activated. However, if more reinforcement particles are added beyond a certain limit, the slope becomes nearly parallel to that of the Hall–Petch line shown as the solid trend lines in Fig. 3b. This implies that the strength increase is merely dominated by the grain refinement and other strengthening routes are essentially deactivated. For the SiC composites in Ref. [45], the initial σ_y is much higher, but $\Delta\sigma_y$ is mostly governed by the grain refinement mechanism without considerable contribution from other strengthening mechanisms. From these results, it is thought that adding nano-sized particles beyond a few vol% (e.g., 2–3 vol% for Refs. [39, 50]) would not effectively devote to $\Delta\sigma_y$ from anticipated Orowan strengthening mechanism.

Alloyed Al systems

Now, in Tables 6 and 7, we summarize the currently available data for the mechanical properties of Al alloy MMC (Table 6) and MMNC (Table 7) materials, respectively, along with the information of reinforcement material types, reinforcement contents, reinforcement particle sizes, and matrix grain sizes [17, 25, 70, 71, 86–93]. Because Al alloys generally possess much higher strength compared with pure Al, there is a greater volume of reported data based on Al alloy metal matrices. Various Al alloys including 2024 AA, 356 AA, 6061 AA, 7075 AA, Al-Cu alloy, etc., have been utilized as the base metal matrices. Because of the general aspects for the

impacts of reinforcement particle volume fractions, particle sizes, and matrix grain sizes on σ_y, σ_{us}, and ε_f of Al alloy MMCs/MMNCs, the Al alloy system sections were simply divided into MMC and MMNC, and results based on the collective data sets are discussed in this section.

MMCs

In Al alloy MMC systems, it is claimed that as the volume fraction of reinforcement particles increases, the interfacial area between the particulates and the matrix increases and more load can be transferred from the matrix to the reinforcement particles, thereby improving σ_y and σ_{us} of the composites. Similar to pure Al systems, further increase in the reinforcement contents may lead to a reduction in the strength of alloyed Al composites, which could be the results of greater agglomeration of particles and a higher degree of defects/micro-porosity formation [93]. For example, Slipenyuk et al.'s [63] research on the SiC/Al composites showed a maximum σ_y at 10 vol% of 3-μm SiC particulates, and reduction in the σ_y values was observed when more reinforcements were added. The critical concentration of reinforcements was found to be greater for the composites containing larger reinforcements, i.e., 14-μm SiC, which also confirms the general trend of the particle size effects discussed for the pure Al systems. As another example, σ_y and σ_{us} started decreasing at higher SiC contents (i.e., beyond 7 vol%) in SiC/Al composites studied in Ref. [65] mostly due to the increased degree of particulate clustering. The composites produced in this work exhibited heterogeneous microstructures with elongated clusters of particles along the extrusion direction, and the local volumes of these clusters varied between 16% for 3 vol% SiC, 12% for 5 vol% of SiC, and 32% for 10 vol% SiC samples, respectively [65]. In Table 6, the SiC/Al composites examined in Ref. [63] present relatively high σ_y and σ_{us}, which can be explained by the effects of post-processing (i.e., aging, age hardening, precipitation hardening) steps in synthesizing the samples. The formation of finely dispersed precipitates in the alloys was the goal of the precipitation hardening process; however, measured ε_f for these composites showed a substantial reduction.

As discussed earlier for pure Al composite materials, for a given particulate volume fraction in a composite system, a clear relationship between the particulate size and σ_y and/or σ_{us} can be identified in alloyed Al systems as well, a decreasing trend with increasing particulate size. For example, the composites reinforced with 16 μm Al_2O_3 in Ref. [73] showed the greatest tensile strength compared with the results from the composites reinforced with 32- and/or 66-μm Al_2O_3 particles. Doel et al. [64] found only a minor difference in σ_y and σ_{us} of the 5- and 13-μm SiC-reinforced composites, but the authors observed that the 60-μm particulate-reinforced materials exhibited much lower σ_y and σ_{us}. A larger ceramic reinforcement particle is more susceptible to fracture at a given applied stress because it is likely to contain a higher quantity of defects larger than critical size. Moreover, it is expected that damaged 60-μm particle would introduce larger-sized flaws or defects within the microstructures and the increase in the stress over the rest of composites for the system with 60-μm particles is likely to be much higher [64]. Therefore, synthesizing composites incorporating smaller particle sizes could provide higher strength and better fabricability as long as the reinforcement concentration does not exceed a certain critical value. We note that the effects of alloy matrix grain sizes on the mechanical properties are not readily available for Al alloy MMC systems because many of the prior studies do not contain the details for the measured grain sizes of metal matrix as shown (i.e., blank data) in Table 6.

Figure 4 epitomizes typical examples of mechanical property changes with (a) reinforcement fractions and (b) yield strength increase ($\Delta\sigma_y$) for collectively selected Al alloy MMC materials from Table 6. Here, we particularly selected the data sets to include ε_f measurements, because the strength and elongation data are both important for practical application of MMC materials. In Fig. 4a, collective data variations for $\Delta\sigma_y$, $\Delta\sigma_{us}$, and $\Delta\varepsilon_f$ as a function of added reinforcement fractions are presented as indicated by the orange, green, and purple symbols, respectively. Vol% or wt% were mixedly used in the plot depending on the units reported in the corresponding literatures. The reinforcement contents were set as the major variable to affect mechanical properties in the results of Fig. 4a, because it is recognized as the prime consideration in synthesizing MMC. Although there are some scatters due to the nature of collective data sets irrespective of processing methods and microstructural features, the $\Delta\sigma_y$, $\Delta\sigma_{us}$, and $\Delta\varepsilon_f$ variations shown in the figure clearly elucidate the

Table 7 Reinforcement types, processing methods, microstructural features, and mechanical properties of Al alloy MMNC systems

Reinforcement types [Ref]	Alloy types	Processing methods/conditions	Reinforcement		Grain size, D (μm)	Mechanical properties			
			Volume fraction (vol%)	Particle size (nm)		E (GPa)	σ_y (MPa)	σ_{us} (MPa)	ε_f (%)
SiC [87]	356 AA	BM + stir casting	0	50	48		122	145	6
			0.5		35		125	219	3.8
			1.5		20		133	238	3.8
			2.5		18		142	257	3.8
			3.5		17		145	285	3.7
			4.5		16		135	241	3.6
SiC [88]	356 AA	Stir casting	0	50	16		71	145	
			0.5				80	200	
			1.5				105	220	
			2.5				120	245	
			3.5				145	270	
			4.5				110	230	
SiC [89]	6061 AA	PM + extrusion	0 (wt%)	500	10	68.5	131	205	16.5
			10 (wt%)			87	192	287	15
			15 (wt%)			103	229	329	14
		PM + heat treatment				69.5	226	342	20.5
						90	281	424	17
						99	307	449	15.5
SiC–B_4C [90]	6061 AA	Casting	0–0			70	70	90	6.1
			0.5–0.5			190	188	217	5.7
			1.0–0.5			200	220	236	5.0
			1.5–0.5			170	193	207	3.5
Al_2O_3 [70]	356 AA	Stir casting	1	50				550.80 (C)	
			2					586.39 (C)	
			3					610.30 (C)	
Al_2O_3 [17]	2024 AA	BM + stir casting	0.0 (wt%)	65	25		85	153	1.3
			0.5 (wt%)				139	190	1.2
			1.0 (wt%)				155	210	0.9
			1.5 (wt%)				150	205	0.7
			2.0 (wt%)				145	200	0.5

Table 7 continued

Reinforcement types [Ref]	Alloy types	Processing methods/conditions	Reinforcement		Grain size, D (μm)	Mechanical properties			
			Volume fraction (vol%)	Particle size (nm)		E (GPa)	σ_y (MPa)	σ_{us} (MPa)	ε_f (%)
Al_2O_3 [91]	356 AA	A356	1.5	20	48	–	130	137	0.70
		Al–4-min stirring			12	79	190	213	0.91
		Al–8-min stirring			14	69	145	182	1.2
		Al–12-min stirring			14	68	150	168	0.58
		Al–16-min stirring			16	61	120	142	0.5
		Cu–4-min stirring			27	88	230	265	1.12
		Cu–8-min stirring			27	78	190	197	0.7
		Cu–12-min stirring			30	71	170	188	0.7
		Cu–16-min stirring			30	61	130	139	0.5
Al_2O_3 [71]	356 AA	Casting	0 (wt%)	300			90 (C)	213.56 (C)	
			1 (wt%)				155 (C)	374.81 (C)	
Al_2O_3 [72]	356 AA	Compocasting	0				83	134	1.55
			1				95	148	1.37
			2				105	153	1.29
			3				111	160	1.19
			4				106	155	0.74
		Stir casting	0				83	134	1.55
			1				86	144	1.31
			2				98	152	1.21
			3				100	150	1.12
Al_2O_3 [92]	356 AA	BM	0	50	48		93	115	2.9
			0.75		16		112	167	2
			1.5		12		116	182	2.2
			2.5		15		113	171	2
			3.5		14		111	163	1.9
			5		15		110	160	1.7
Al_2O_3 [93]	6061 AA	As cast	0	40			85	110	
			0.5				175	212	
			1.0				250	260	
			1.5				200	210	
		Extrusion		40			160	195	
							210	250	
							270	305	
							345	375	

Table 7 continued

Reinforcement types [Ref]	Alloy types	Processing methods/conditions	Reinforcement		Grain size, D (μm)	Mechanical properties			
			Volume fraction (vol%)	Particle size (nm)		E (GPa)	σ_y (MPa)	σ_{us} (MPa)	ε_f (%)
ZrO_2 [25]	LM13 AA	Melt deposition hot extrusion	0 (wt%)	50–80			120	170	11
			3 (wt%)				124	230	7.4
			6 (wt%)				132	248	5.8
			9 (wt%)				158	257	5.0
			12 (wt%)				183	262	4.2
			15 (wt%)				171	258	3.5
TiB_2 [86]	356 AA	Stir casting	0	20		70.73	237	242.6	
			0.5			83.11	241	333.2	
			1.5			82.85	277	364.9	
			3.0			78.82	258	310	
			5.0			78.31	241	283	

contemporary status of Al alloy MMC materials. From a collective point of view, reinforcement particles may be added up to ~20 and ~7–8 vol% (or wt%) to increase σ_y and σ_{us}, respectively, but adding larger amounts of particulates can substantially decrease ε_f. In fact, all results containing more than 20% of reinforcements suffered from more than 50% reduction in ε_f. The collective property change data with $\Delta\sigma_y$ variations given in Fig. 4b clearly confirm this; when $\Delta\sigma_y$ is greater than 60%, ε_f of the sample essentially approaches to 0 by losing at least 70% of original elongation ability. For instance, in Ref. [63], $\Delta\sigma_y = 83.44\%$ in the Al-Cu sample with addition of 20 vol% SiC is compensated by $\Delta\varepsilon_f = -92.46\%$. σ_{us} may increase as σ_y increases by ~50%; however, a decreasing trend in relative $\Delta\sigma_{us}$ is apparent when σ_y increases beyond ~50%. It is considered that minimization of such sacrifice in $\Delta\sigma_{us}$ and $\Delta\varepsilon_f$ with high $\Delta\sigma_y$ is still a formidable challenge in developing advanced high-strength high-ductility Al MMC systems.

The ultimate intent of developing MMC materials is to enhance the mechanical performance of composites starting from the monolithic metal matrix. Therefore, it is of pivotal importance to assess how much improvements can be made from the monolithic metal matrix by adding reinforcements. In Fig. 5, we present the variations of (a) $\Delta\sigma_y$, (b) $\Delta\sigma_{us}$, and (c) $\Delta\varepsilon_f$ as a function of respective monolithic properties for Al alloy MMCs using the same data sets included in Fig. 4. Symbols with identical types and colors have been used to denote the same specimen. For $\Delta\sigma_y$ case, the majority of testing samples exhibited $\Delta\sigma_y$ values under ~30–40% and maximum $\Delta\sigma_y$ was observed when the σ_y of monolithic metal matrix is near ~150 MPa. However, such maximum $\Delta\sigma_y$ reported in Al-Cu alloys in Ref. [63] is thought to be the results of heat treatment and aging rather than those of particulate incorporation. The 356 AA composites reinforced with SiC-RHA (rice husk ash) studied in Ref. [69] showed a decent combination of $\Delta\sigma_y$ (=53.57%) and $\Delta\varepsilon_f$ (=−33.33%). Other than these two examples, generally, it is summarized that $\Delta\sigma_y$ could be achieved up to a maximum of ~30–40% over the entire range of starting monolithic σ_y. From the figure, one can apparently notice that the $\Delta\sigma_{us}$ variations with starting σ_{us} are much smaller than $\Delta\sigma_y$ variations and that some of σ_{us} exhibited even lower values than the original monolithic σ_{us}. In the data set

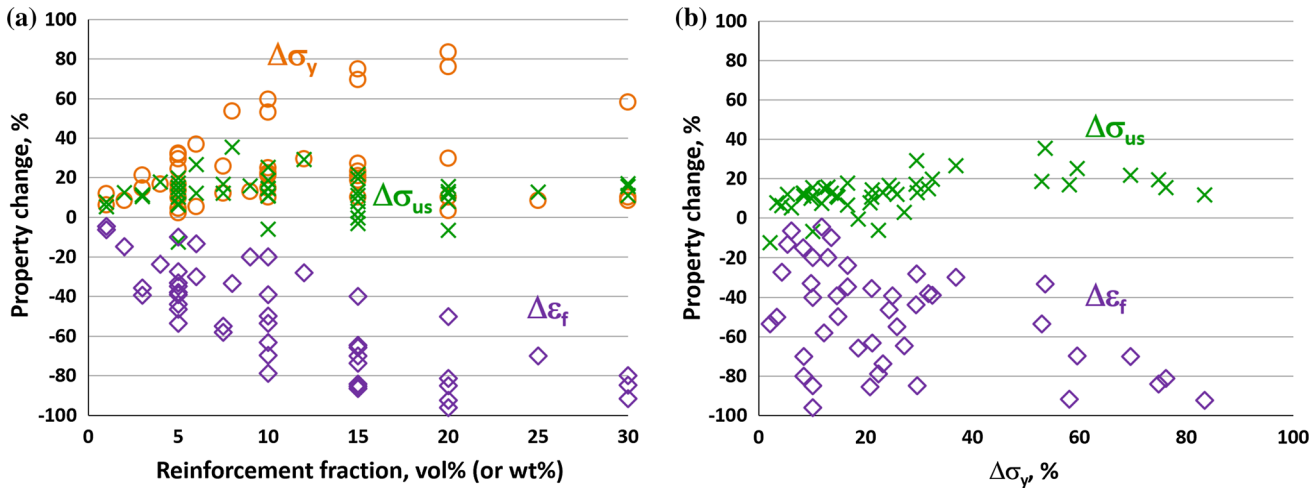

Figure 4 Mechanical property changes with **a** reinforcement fractions and **b** $\Delta\sigma_y$ for Al alloy MMC systems.

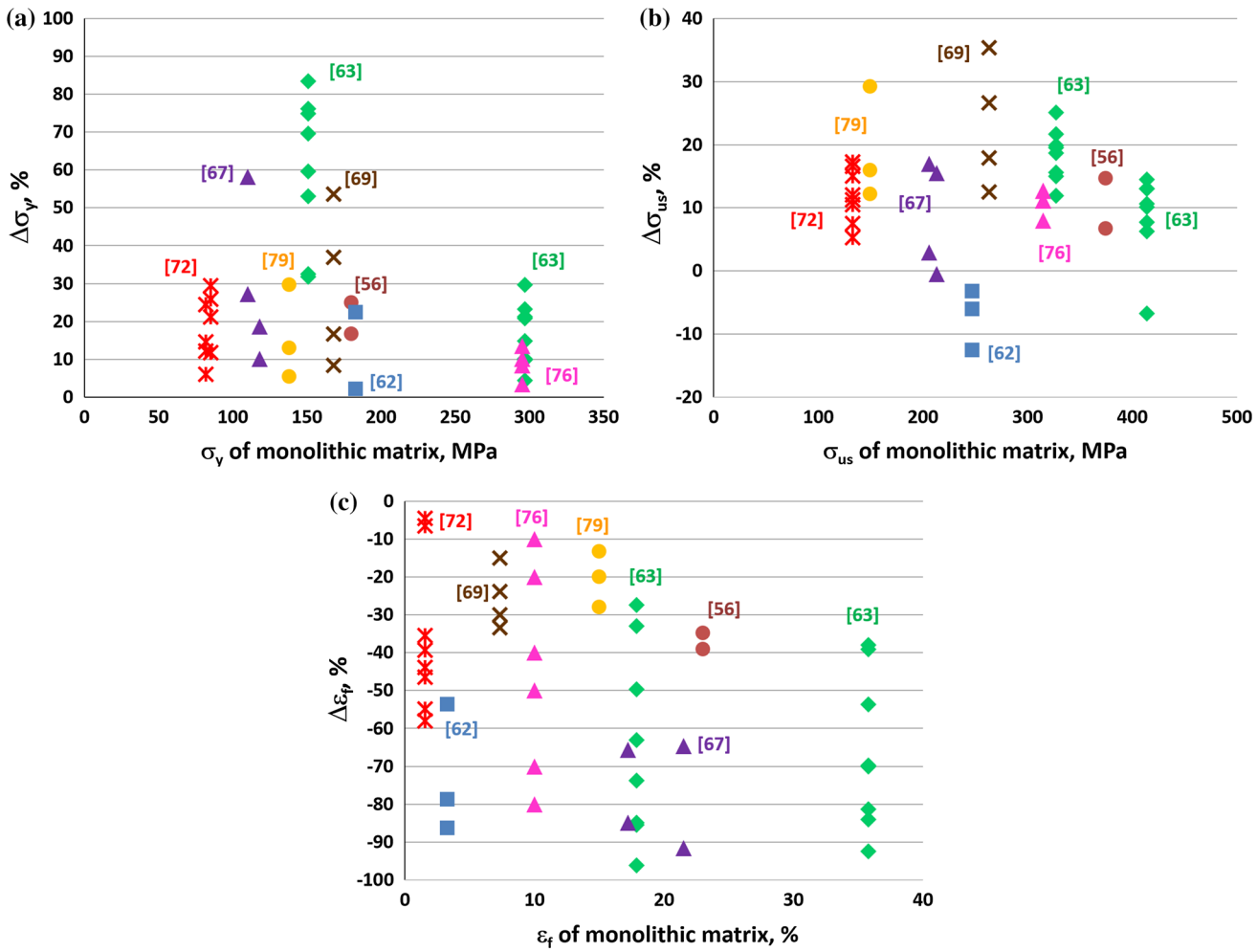

Figure 5 Variations of **a** $\Delta\sigma_y$, **b** $\Delta\sigma_{us}$, and **c** $\Delta\varepsilon_f$ as a function of respective monolithic properties for Al alloy MMC systems.

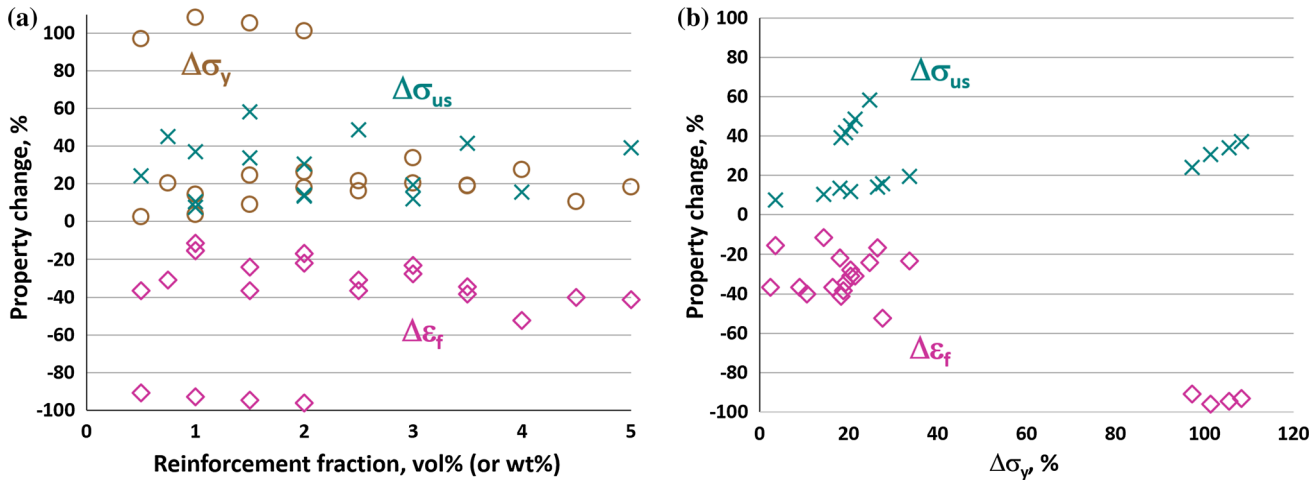

Figure 6 Mechanical property changes with **a** reinforcement fractions and **b** $\Delta\sigma_y$ for Al alloy MMNC systems.

shown in Fig. 5b, maximum $\Delta\sigma_{us}$ was found in the samples to contain SiC-RHA reinforcements started from $\sigma_{us} = 263$ MPa [69]. $\Delta\sigma_{us}$ reported in Bharath et al.'s [79] work also showed a relatively high value ($\Delta\sigma_{us} = 29.59\%$) when 12 vol% of Al_2O_3 was added to 6061 AA. From the figure, $\Delta\sigma_{us}$ is typically measured smaller than ~20%. Although the $\Delta\varepsilon_f$ variations with initial monolithic ε_f are widely spread out, the scatter plots displayed in Fig. 5c generally confirm that ε_f of composites is greatly reduced when the monolithic ε_f is large; if the starting ε_f is greater than 20%, $\Delta\varepsilon_f$ of alloyed Al MMC systems unanimously experienced higher degrees of reduction more than −30%. In Fig. 5c, the relatively smaller $\Delta\varepsilon_f$ (less than −30%) is mostly correlated with the smaller amount of reinforcement addition and therefore smaller $\Delta\sigma_y$. We must again note that although the collective data sets contained in Figs. 4 and 5 are based on the selected experimental measurements listed in Table 6 that contain ε_f information, they clearly elucidate the current status of Al alloy MMC systems regarding the improvements of three important mechanical properties, i.e., $\Delta\sigma_y$, $\Delta\sigma_{us}$, and $\Delta\varepsilon_f$.

MMNCs

In general, a similar trend for the effects of particle volume fractions on the mechanical properties is observed for Al alloy MMNC; there is a certain critical value where nano-composites exhibit their maximum σ_y and σ_{us}. It was claimed that such critical volume fraction is the point where the matrix is particle-saturated and that further addition of the particulate volume fraction would not impose substantial impacts on the grain size of the matrix; therefore, the grain refinement effects remain independent of the particulate volume fraction beyond this critical point [93]. For instance, it was found that additional increase of Al_2O_3 reinforcement contents beyond 3 wt% caused a reduction in σ_y in Sajjadi et al.'s [72] study. The authors showed that higher degrees of particle agglomeration, defects, and microporosity were observed with higher contents of Al_2O_3 reinforcements. As an exception for this trend, the SiC/Al nano-composites in Ref. [89] exhibited monotonous increase in σ_y and σ_{us} with reinforcement additions up to 15 wt%. It is considered that the low-temperature aging treatment chosen (125 °C for 8 h) in this work improved the mechanical property values. The authors claimed that because of homogeneous particle distribution without a significant clustering, no peaks were found in σ_y and σ_{us} of these composites [89]. However, the SiC particle size embedded in the composites was < 500 nm, which is relatively larger than the dimension of typical nano-sized ceramic particulates (i.e., < ~100 nm). We also find that ε_f in general gradually decreases with increasing the contents of nano-sized particles. Besides greater agglomeration, the increased mass fraction of nanoparticles will decrease the effective slip distance of dislocations during deformation, which will in turn decrease ε_f [94, 95].

In Fig. 6, the collective mechanical property changes with (a) reinforcement fractions and (b) $\Delta\sigma_y$ for Al

alloy MMNCs are summarized. Again, the currently available data sets to contain ε_f measurements have been included in the figure. As shown in Fig. 6, the numbers of Al alloy MMNC data sets to report ε_f values are limited because many of the prior literatures primarily focused only on the strength improvement ignoring ε_f. Here, it is first noticed that much smaller reinforcement fractions are added in MMNCs, i.e., up to ~5 vol% (or wt%), because of higher propensity for particle agglomeration due to the greater instability of nano-sized particulates embedded in MMNC. From Fig. 6a, most of the MMNC specimen exhibit $\Delta\sigma_y$ and $\Delta\sigma_{us}$ values under ~40%. $\Delta\sigma_{us}$ and $\Delta\varepsilon_f$ are generally expected to increase and decrease with increasing $\Delta\sigma_y$ for Al alloy MMNC systems as well, but the scatter data shown in Fig. 6b do not clearly show such trend partly due to the lack of available data sets and partly due to the variety of processing techniques in synthesizing MMNC materials.

In addition to the property changes with reinforcement fractions and $\Delta\sigma_y$, in Fig. 7, we present the collective data of (a) $\Delta\sigma_y$, (b) $\Delta\sigma_{us}$, and (c) $\Delta\varepsilon_f$ as a function of respective monolithic properties for Al alloy MMNC. Again, identical types and colors of symbols have been used to indicate the same alloyed Al MMNC samples. The 2024 AA composites reinforced with Al_2O_3 prepared by Su et al. [17] showed much improvements (nearly ~100% or higher) for $\Delta\sigma_y$, but these samples have been subjected to a substantial decrease in ε_f (nearly ~100%) as evidenced in Fig. 7c. Such ε_f loss can stem from the excessive generation of dislocations during the ball-milling process applied to synthesize the samples. On

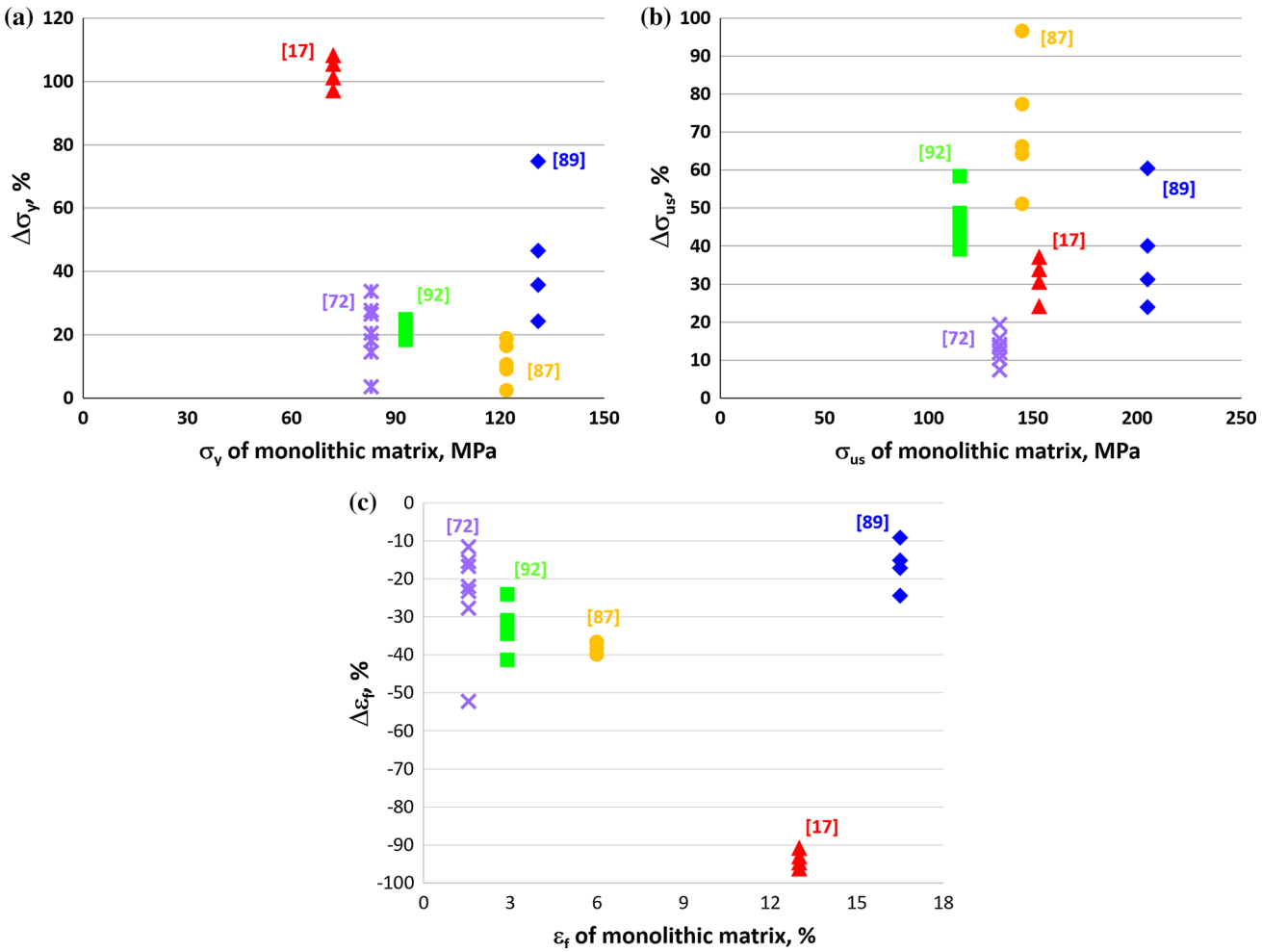

Figure 7 Variations of **a** $\Delta\sigma_y$, **b** $\Delta\sigma_{us}$, and **c** $\Delta\varepsilon_f$ as a function of respective monolithic properties for Al alloy MMNC systems.

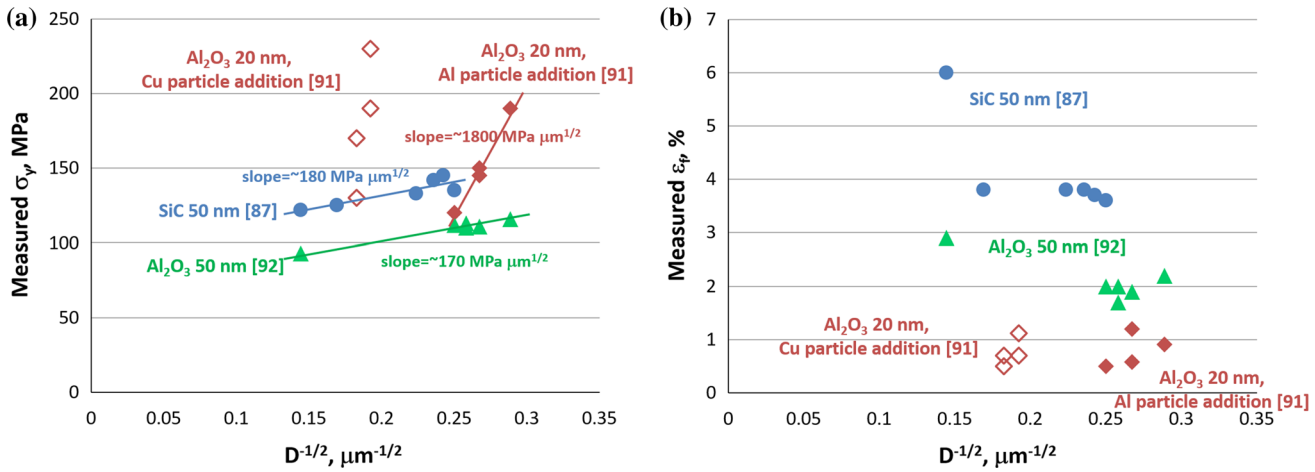

Figure 8 Variations of experimental **a** σ_y and **b** ε_f with the inverse of square root of matrix grain sizes ($D^{-1/2}$) for Al alloy MMNCs (356 AA).

the other hand, when $\Delta\sigma_y$ is relatively small, corresponding $\Delta\varepsilon_f$ was also small as shown in the example of Ref. [72]. Out of the alloyed Al MMNC materials in Table 7, the 6061 AA systems with 500-nm particles studied by Knowles et al. [89] exhibited a decent combination of $\Delta\sigma_y = 74\%$, $\Delta\sigma_{us} = 60\%$, and $\Delta\varepsilon_f = -15\%$. Except the $\Delta\varepsilon_f$ values reported in Ref. [89], similar to the Al alloy MMC systems shown in Fig. 5c, we again find that generally ε_f loss of composites is larger when the monolithic ε_f is larger, which implies that we may lose nearly all ductility of alloyed Al MMNC materials even starting from relatively ductile metal matrix.

As mentioned earlier, there is an obvious impact of reinforcement material types and contents on the matrix grain sizes of composites, and the grain sizes of matrix can play an important role in determining mechanical properties of final polycrystalline products. Figure 8 illustrates the selected examples of (a) σ_y and (b) ε_f variations as a function of metal-matrix grain sizes for alloyed Al MMNCs listed in Table 7. In Ref. [91], reduced matrix grain sizes were observed by adding more Al_2O_3 particles, and consequently the flow stress of the composite was found to increase with greater contents of Al_2O_3 particles in the composites. With higher Al_2O_3 contents, the Al metal matrix experiences considerable constraints to the plastic deformation due to smaller inter-particle distance and finer matrix grain sizes. SiC particles have shown similar effects on the matrix grain size, where grain refinement strengthening effects were identified in Mazahery et al.'s [87] work. In their study, the grain refinement strengthening mechanism was greatly evidenced with increasing particulate volume fraction because the reinforcement particles can serve as the heterogeneous nucleation catalyst [87]. When the slopes of σ_y vs. $D^{-1/2}$ are quantified, the values are regressively approximated as ~180, ~170, and ~1800 MPa $\mu m^{1/2}$ for the samples of Refs. [87], [92], and [91], respectively. Here, the data set for the samples synthesized with adding Cu particles [i.e., open symbols in Fig. 8a] has not been analyzed. Recognizing that the Hall–Petch constant (k_y) is ~160–170 MPa $\mu m^{1/2}$ for 356 AA alloys [96], $\Delta\sigma_y$ occurred in the composites of Refs. [87] and [92] is mostly governed by the grain refinement effects, not by the Orowan strengthening mechanism. On the other hand, it seems that $\Delta\sigma_y$ in Ref. [91] was attained by activating other strengthening mechanisms such as Orowan or solid solution hardening mechanisms. As for ε_f, it is noticed that ε_f is generally decreased with decreasing grain sizes as shown in Fig. 8b. Such reduction in ε_f with adding nano-sized particles and resultant smaller grain sizes is clearly reported in the samples of Refs. [87] and [92]. The 356 AA materials reinforced with Al_2O_3 nanoparticles and Al (or Cu) exhibited relatively high σ_y; however, the ε_f values of these samples were minimal irrespective of the matrix grain sizes.

From Tables 6 and 7, we find that maximum σ_y of Al alloy MMC is 385 MPa in an Al-20 vol% SiC MMC [63], while maximum σ_y of Al alloy MMNCs is 307 MPa in an Al-15 wt% SiC MMNC [89]. When the strength increase is considered for these systems, 88 and 81 MPa of σ_y were improved, respectively. As for σ_{us}, Al/10 vol% Al_2O_3 MMC with an ultimate tensile

strength of 482.5 MPa [74] exhibited the highest value among the Al alloy MMC systems, and Al/15 wt% SiC MMNC with a maximum ultimate tensile strength of 449 MPa [89] was the best out of the alloyed Al MMNC samples. Generally speaking, $\Delta\sigma_y$ and $\Delta\sigma_{us}$ are expected in the range of less than $\sim$40 and $\sim$20% both for Al alloy MMC and MMNC materials. Some samples showed much enhanced strength, but they typically exhibited a substantial reduction in their ductility, implying that the strengthening mechanism is originated from the generation of extensive dislocations upon processing, not from the activation of desired load transfer or Orowan strengthening mechanisms. The situations for pure Al MMC and MMNC materials are similar to those for alloyed Al MMC/MMNC. Because the intrinsic material properties of pure Al are more ductile with a lower strength value, σ_y and σ_{us} of pure Al could be increased much more than the alloyed Al composite cases; however, the impacts of adding nano-sized reinforcement particulates are not prominent. Therefore, it is thought that, based on the collected data from existing literature, not a substantial difference between the mechanical performances of the Al MMCs and Al MMNCs samples was found by adding micron-sized or nano-sized particulates both from the absolute and the relative strength increase point of views. Although there has been a discernable progress in the field of particulate-reinforced Al MMCs/MMNCs, the synthesized products still show relatively low ductility and ε_f. More in-depth understanding for the relationship among the processing, microstructure, and mechanical performance will be necessary to minimize such inferior ductility of Al MMC/MMNC composites. It is anticipated that the benefit of adding nano-sized reinforcements could be maximized by developing more advanced synthesis techniques such as near-net shape, in situ fabrications [97–100] and by applying more adequate heat treatments that can prevent the agglomeration and aid the homogeneous distribution of reinforcement particulates.

Summary

In the present study, we have thoroughly analyzed the mechanical performance of pure Al MMC/MMNC and alloyed Al MMC/MMNC systems using a comprehensive collection of currently available data sets. The analysis includes the effects of the particle volume fractions, particle sizes, and matrix grain sizes on the σ_y, σ_{us}, and ε_f variations of composites. Results showed that the reinforcement particulate contents directly affect σ_y, σ_{us}, and ε_f of pure and alloyed Al MMC/MMNC. Depending on the fabrication process, particle size ratio (PSR), and post-processing treatments and heat treatments, an optimum particle volume fraction exists where maximum σ_y and σ_{us} are observed. Although the metal-matrix grain size is one of the most basic parameters to determine the mechanical properties of Al MMC/MMNC, adequate measurements for the grain sizes have not been conducted in many previous studies. Addition of reinforcements clearly reduced the ductility of monolithic metal matrix, and the degree of losing ductility was generally found to be greater as the initial ductility of monolithic matrix is higher. While one may expect to attain significant advantages of adding nano-sized reinforcements over the micron-sized reinforcements, not a clear benefit to incorporate nano-sized particulate is identified in the mechanical performance improvements for particulate-reinforced Al-based composite systems. Although there are certain limitations in the mechanical performance of contemporary Al-based MMNC materials, in the future, developing more advanced Al-based MMNC materials is highly expected by applying innovative synthesis techniques along with relevant heat treatments.

Acknowledgements

This material is based upon work supported by the US Army Research Laboratory under Cooperative Agreement No. W911NF-15-20005. The views, opinions, and conclusions made in this document are those of authors and should not be interpreted the official policies, either expressed or implied, of Army Research Laboratory or the US Government. The US Government is authorized to reproduce and distribute reprints for Government purposes notwithstanding any copyright notation herein.

References

[1] Rohatgi PK, Asthana R, Das S (1986) Solidification, structures, and properties of cast metal-ceramic particle composites. Int Metals Rev 31(1):115–139

[2] Stefanescu DM, Dhindaw BK, Kacar SA, Moitra A (1988) Behavior of ceramic particles at the solid-liquid metal interface in metal matrix composites. Metall Trans A 19(11):2847–2855

[3] Ferguson JB, Thao X, Rohatgi PK, Cho K, Kim CS (2014) Computational and analytical prediction of the elastic modulus and yield stress in particulate-reinforced metal matrix composites. Scripta Mater 83:45–48

[4] Srinivasarao B, Suryanarayana C, Oh-Ishi K, Hono K (2009) Microstructure and mechanical properties of Al–Zr nanocomposite materials. Mater Sci Eng A 518(1):100–107

[5] Breslin MC, Ringnalda J, Xu L, Fuller M, Seeger J, Daehn GS, Otani T, Fraser HL (1995) Processing, microstructure, and properties of co-continuous alumina–aluminum composites. Mater Sci Eng A 195:113–119

[6] Halverson DC, Pyzik AJ, Aksay IA, Snowden WE (1989) Processing of boron carbide-aluminum composites. J Am Ceram Soc 72(5):775–780

[7] Nardone VC, Prewo KM (1986) On the strength of discontinuous silicon carbide reinforced aluminum composites. Scripta Mater 20(1):43–48

[8] Prasad SV, Asthana R (2004) Aluminum metal-matrix composites for automotive applications: tribological considerations. Tribol Lett 17(3):445–453

[9] Rawal SP (2001) Metal-matrix composites for space applications. JOM 53(4):14–17

[10] Aghajanian MK, Rocazella MA, Burke JT, Keck SD (1991) The fabrication of metal matrix composites by a pressureless infiltration technique. J Mater Sci 26(2):447–454. doi:10.1007/BF00576541

[11] Clyne TW, Mason JF (1987) The squeeze infiltration process for fabrication of metal-matrix composites. Metall Trans A 18(8):1519–1530

[12] Hashim J, Looney L, Hashmi MS (1999) Metal matrix composites: production by the stir casting method. J Mater Process Technol 92:1–7

[13] Kong CY, Soar RC (2005) Fabrication of metal–matrix composites and adaptive composites using ultrasonic consolidation process. Mater Sci Eng A 412(1):12–18

[14] Min SO (2009) Effects of volume fraction of SiC particles on mechanical properties of SiC/Al composites. Trans Nonferrous Met Soc China 19(6):1400–1404

[15] Koli DK, Agnihotri G, Purohit R (2014) A review on properties, behaviour and processing methods for Al-nano Al_2O_3 composites. Procedia Mater Sci 6:567–589

[16] Rahimian M, Parvin N, Ehsani N (2011) The effect of production parameters on microstructure and wear resistance of powder metallurgy Al–Al_2O_3 composite. Mater Des 32(2):1031–1038

[17] Su H, Gao W, Feng Z, Lu Z (2012) Processing, microstructure and tensile properties of nano-sized Al_2O_3 particle reinforced aluminum matrix composites. Mater Des 36:590–596

[18] Huang X, Kamikawa N, Hansen N (2008) Strengthening mechanisms in nanostructured aluminum. Mater Sci Eng A 483:102–104

[19] Shanmugasundaram T, Heilmaier M, Murty BS, Sarma VS (2010) On the Hall-Petch relationship in a nanostructured Al–Cu alloy. Mater Sci Eng A 527(29):7821–7825

[20] Weertman JR (1993) Hall-Petch strengthening in nanocrystalline metals. Mater Sci Eng A 166(1–2):161–167

[21] Zhang Z, Chen DL (2008) Contribution of Orowan strengthening effect in particulate-reinforced metal matrix nanocomposites. Mater Sci Eng 483:148–152

[22] Yar AA, Montazerian M, Abdizadeh H, Baharvandi HR (2009) Microstructure and mechanical properties of aluminum alloy matrix composite reinforced with nano-particle MgO. J Alloys Compd 484(1):400–404

[23] Arsenault RJ (1991) Strengthening mechanisms in particulate MMC: remarks on a paper by Miller and Humphreys. Scripta Mater 25(11):2617–2621

[24] Miller WS, Humphreys FJ (1991) Strengthening mechanisms in particulate metal matrix composites. Scripta Mater 25(1):33–38

[25] Hemanth J (2009) Development and property evaluation of aluminum alloy reinforced with nano-ZrO_2 metal matrix composites (NMMCs). Mater Sci Eng A 507(1):110–113

[26] Hall JN, Jones JW, Sachdev AK (1994) Particle size, volume fraction and matrix strength effects on fatigue behavior and particle fracture in 2124 aluminum-SiC p composites. Mater Sci Eng A 183(1):69–80

[27] Mortensen A, Llorca J (2010) Metal matrix composites. Annu Rev Mater Res 40:243–270

[28] Rajan TP, Pillai RM, Pai BC (1998) Reinforcement coatings and interfaces in aluminum metal matrix composites. J Mater Sci 33(14):3491–3503. doi:10.1023/A:1004674822751

[29] Kang CG, Lee JH, Youn SW, Oh JK (2005) An estimation of three-dimensional finite element crystal geometry model for the strength prediction of particle-reinforced metal matrix composites. J Mater Process Technol 166(2):173–182

[30] Xu N, Zong BY (2008) Stress in particulate reinforcements and overall stress response on aluminum alloy matrix composites during straining by analytical and numerical modeling. Comput Mater Sci 43(4):1094–1100

[31] Engberg CJ, Zehms EH (1959) Thermal expansion of Al_2O_3, BeO, MgO, B_4C, SiC, and TiC Above 1000°. C J Am Ceram Soc 42(6):300–305

[32] Waku Y, Nakagawa N, Wakamoto T, Ohtsubo H, Shimizu K, Kohtoku Y (1998) High-temperature strength and thermal stability of a unidirectionally solidified Al_2O_3/YAG eutectic composite. J Mater Sci 33(5):1217–1225. doi:10.1023/A:1004377626345

[33] Hashim J, Looney L, Hashmi MS (2001) The wettability of SiC particles by molten aluminium alloy. J Mater Process Technol 119(1):324–328

[34] Sarina BA, Kai TA, Kvithyld A, Thorvald EN, Tangstad M (2012) Wetting of pure aluminium on graphite, SiC and Al_2O_3 in aluminium filtration. Trans Nonferrous Met Soc China 22(8):1930–1938

[35] Ibrahim IA, Mohamed FA, Lavernia EJ (1991) Particulate reinforced metal matrix composites—a review. J Mater Sci 26(5):1137–1156. doi:10.1007/BF00544448

[36] Leon-Patino CA, Drew RA (2005) Role of metal interlayers in the infiltration of metal–ceramic composites. Curr Opin Solid State Mater Sci 9(4):211–218

[37] Tan M, Xin Q, Li Z, Zong BY (2001) Influence of SiC and Al_2O_3 particulate reinforcements and heat treatments on mechanical properties and damage evolution of Al-2618 metal matrix composites. J Mater Sci 36(8):2045–2053. doi:10.1023/A:1017591117670

[38] Lloyd DJ (1994) Particle reinforced aluminium and magnesium matrix composites. Int Mater Rev 39(1):1–23

[39] Kang YC, Chan SL (2004) Tensile properties of nanometric Al_2O_3 particulate-reinforced aluminum matrix composites. Mater Chem Phys 85(2):438–443

[40] Sun C, Song M, Wang Z, He Y (2011) Effect of particle size on the microstructures and mechanical properties of SiC-reinforced pure aluminum composites. J Mater Eng Perform 20(9):1606–1612

[41] Rahimian M, Ehsani N, Parvin N, reza Baharvandi H (2009) The effect of particle size, sintering temperature and sintering time on the properties of Al–Al_2O_3 composites, made by powder metallurgy. J Mater Process Technol 209(14):5387–5393

[42] Rahimian M, Parvin N, Ehsani N (2010) Investigation of particle size and amount of alumina on microstructure and mechanical properties of Al matrix composite made by powder metallurgy. Mater Sci Eng A 527(4):1031–1038

[43] Rezayat M, Akbarzadeh A, Owhadi A (2012) Production of high strength Al– Al_2O_3 composite by accumulative roll bonding. Compos A 43(2):261–267

[44] Ahmadi A, Toroghinejad MR, Najafizadeh A (2014) Evaluation of microstructure and mechanical properties of Al/Al_2O_3/SiC hybrid composite fabricated by accumulative roll bonding process. Mater Des 53:13–19

[45] Kamrani S, Riedel R, Reihani SS, Kleebe HJ (2009) Effect of reinforcement volume fraction on the mechanical properties of Al-SiC nanocomposites produced by mechanical alloying and consolidation. J Compos Mater

[46] Kollo L, Bradbury CR, Veinthal R, Jäggi C, Carreno-Morelli E, Leparoux M (2011) Nano-silicon carbide reinforced aluminium produced by high-energy milling and hot consolidation. Mater Sci Eng A 528(21):6606–6615

[47] Mula S, Padhi P, Panigrahi SC, Pabi SK, Ghosh S (2009) On structure and mechanical properties of ultrasonically cast Al–2% Al_2O_3 nanocomposite. Mater Res Bull 44(5):1154–1160

[48] Khorshid MT, Jahromi SJ, Moshksar MM (2010) Mechanical properties of tri-modal Al matrix composites reinforced by nano-and submicron-sized Al_2O_3 particulates developed by wet attrition milling and hot extrusion. Mater Des 31(8):3880–3884

[49] Sharifi EM, Karimzadeh F, Enayati MH (2011) Fabrication and evaluation of mechanical and tribological properties of boron carbide reinforced aluminum matrix nanocomposites. Mater Des 32(6):3263–3271

[50] Alizadeh M (2014) Strength prediction of the ARBed Al/Al_2O_3/B 4 C nano-composites using Orowan model. Mater Res Bull 59:290–294

[51] Fathy A, Sadoun A, Abdelhameed M (2014) Effect of matrix/reinforcement particle size ratio (PSR) on the mechanical properties of extruded Al–SiC composites. Int J Adv Manuf Technol 73(5–8):1049–1056

[52] El-Kady O, Fathy A (2014) Effect of SiC particle size on the physical and mechanical properties of extruded Al matrix nanocomposites. Mater Des 54:348–353

[53] Ferguson JB, Lopez HF, Rohatgi PK, Cho K, Kim CS (2014) Impact of volume fraction and size of reinforcement particles on the grain size in metal–matrix micro and nanocomposites. Metall Mater Trans A 45(9):4055–4061

[54] Kim CS, Sohn I, Nezafati M, Ferguson JB, Schultz BF, Bajestani-Gohari Z, Rohatgi PK, Cho K (2013) Prediction models for the yield strength of particle-reinforced unimodal pure magnesium (Mg) metal matrix nanocomposites (MMNCs). J Mater Sci 48(12):4191–4204. doi:10.1007/s10853-013-7232-x

[55] Ferguson JB, Schultz BF, Venugopalan D, Lopez HF, Rohatgi PK, Cho K, Kim CS (2014) On the superposition of strengthening mechanisms in dispersion strengthened alloys and metal-matrix nanocomposites: considerations of stress and energy. Met Mater Int 20(2):375

[56] Mondal DP, Das S, Suresh KS, Ramakrishnan N (2007) Compressive deformation behavior of coarse SiC particle reinforced composite: effect of age-hardening and SiC content. Mater Sci Eng A 460:550–560

[57] Wang Z, Song M, Sun C, He Y (2011) Effects of particle size and distribution on the mechanical properties of SiC

reinforced Al–Cu alloy composites. Mater Sci Eng A 528(3):1131–1137

[58] Wang Z, Song M, Sun C, Xiao D, He Y (2010) Effect of extrusion and particle volume fraction on the mechanical properties of SiC reinforced Al–Cu alloy composites. Mater Sci Eng A 527(24):6537–6542

[59] Hua Y, Gu L (2013) Prediction of the thermomechanical behavior of particle-reinforced metal matrix composites. Compos B 45(1):1464–1470

[60] Amirkhanlou S, Rezaei MR, Niroumand B, Toroghinejad MR (2011) High-strength and highly-uniform composites produced by compocasting and cold rolling processes. Mater Des 32(4):2085–2090

[61] Jamaati R, Amirkhanlou S, Toroghinejad MR, Niroumand B (2011) Effect of particle size on microstructure and mechanical properties of composites produced by ARB process. Mater Sci Eng A 528(4):2143–2148

[62] Onat A, Akbulut H, Yilmaz F (2007) Production and characterisation of silicon carbide particulate reinforced aluminium–copper alloy matrix composites by direct squeeze casting method. J Alloys Compd 436(1):375–382

[63] Slipenyuk A, Kuprin V, Milman Y, Goncharuk V, Eckert J (2006) Properties of P/M processed particle reinforced metal matrix composites specified by reinforcement concentration and matrix-to-reinforcement particle size ratio. Acta Mater 54(1):157–166

[64] Doel TJ, Bowen P (1996) Tensile properties of particulate-reinforced metal matrix composites. Compos A 27(8):655–665

[65] Hong SJ, Kim HM, Huh D, Suryanarayana C, Chun BS (2003) Effect of clustering on the mechanical properties of SiC particulate-reinforced aluminum alloy 2024 metal matrix composites. Mater Sci Eng A 347(1):198–204

[66] Suh YS, Joshi SP, Ramesh KT (2009) An enhanced continuum model for size-dependent strengthening and failure of particle-reinforced composites. Acta Mater 57(19):5848–5861

[67] Ogel B, Gurbuz R (2001) Microstructural characterization and tensile properties of hot pressed Al–SiC composites prepared from pure Al and Cu powders. Mater Sci Eng A 301(2):213–220

[68] Rajmohan T, Palanikumar K, Ranganathan S (2013) Evaluation of mechanical and wear properties of hybrid aluminium matrix composites. Trans Nonferrous Met Soc China 23(9):2509–2517

[69] Prasad DS, Shoba C, Ramanaiah N (2014) Investigations on mechanical properties of aluminum hybrid composites. J Mater Res Technol 3(1):79–85

[70] Sajjadi SA, Ezatpour H, Beygi H (2011) Microstructure and mechanical properties of Al–Al_2O_3 micro and nano composites fabricated by stir casting. Mater Sci Eng 528:8765–8771

[71] Hossein-Zadeh M, Mirzaee O, Saidi P (2014) Structural and mechanical characterization of Al-based composite reinforced with heat treated Al_2O_3 particles. Mater Des 54:245–250

[72] Sajjadi SA, Ezatpour HR, Parizi MT (2012) Comparison of microstructure and mechanical properties of A356 aluminum alloy/Al_2O_3 composites fabricated by stir and compo-casting processes. Mater Des 34:106–111

[73] Kok M (2005) Production and mechanical properties of Al_2O_3 particle-reinforced 2024 aluminum alloy composites. J Mater Process Technol 161(3):381–387

[74] Chou SN, Lu HH, Lii DF, Huang JL (2009) Processing and physical properties of Al_2O_3/aluminum alloy composites. Ceram Int 35(1):7–12

[75] Nagaral M, Bharath V, Auradi V (2013) Effect of Al_2O_3 particles on mechanical and wear properties of 6061Al alloy metal matrix composites. J Mater Sci Eng 2

[76] Hauert A, Rossoll A, Mortensen A (2010) Fracture of high volume fraction ceramic particle reinforced aluminium under multiaxial stress. Acta Mater 58(11):3895–3907

[77] Al-Dheylan K, Hafeez S (2006) Tensile failure micro mechanisms of 6061 Aluminum reinforced with submicron Al_2O_3 metal-matrix composites. AJSE Sec B 31(2C):89–98

[78] Park BG, Crosky AG, Hellier AK (2001) Material characterization and mechanical properties of Al_2O_3–Al metal matrix composites. J Mater Sci 36(10):2417–2426. doi10.1023/A:1017921813503

[79] Bharath V, Nagaral M, Auradi V, Kori SA (2014) Preparation of 6061Al- Al_2O_3 MMC's by stir casting and evaluation of mechanical and wear properties. Procedia Mater Sci 6:1658–1667

[80] Kim HH, Babu JS, Kang CG (2013) Fabrication of A356 aluminum alloy matrix composite with CNTs/Al_2O_3 hybrid reinforcements. Mater Sci Eng A 573:92–99

[81] Ramnath BV, Elanchezhian C, Jaivignesh M, Rajesh S, Parswajinan C, Ghias AS (2014) Evaluation of mechanical properties of aluminium alloy–alumina–boron carbide metal matrix composites. Mater Des 58:332–338

[82] Alizadeh M, Paydar MH, Jazi FS (2013) Structural evaluation and mechanical properties of nanostructured Al/B 4 C composite fabricated by ARB process. Compos B 44(1):339–343

[83] Baradeswaran A, Perumal AE (2013) Influence of B4C on the tribological and mechanical properties of Al 7075–B4C composites. Compos B 54:146–152

[84] Rajan HM, Ramabalan S, Dinaharan I, Vijay SJ (2013) Synthesis and characterization of in situ formed titanium diboride particulate reinforced AA7075 aluminum alloy cast composites. Mater Des 44:438–445

[85] Suresh S, Moorthi NS (2013) Process development in stir casting and investigation on microstructures and wear behavior of TiB_2 on Al6061 MMC. Procedia Eng. 64:1183–1190

[86] Akbari MK, Baharvandi HR, Shirvanimoghaddam K (2015) Tensile and fracture behavior of nano/micro TiB 2 particle reinforced casting A356 aluminum alloy composites. Mater Des 66:150–161

[87] Mazahery A, Shabani MO (2012) Characterization of cast A356 alloy reinforced with nano SiC composites. Trans Nonferrous Met Soc China 22(2):275–280

[88] Mazahery A, Shabani MO (2012) Nano-sized silicon carbide reinforced commercial casting aluminum alloy matrix: experimental and novel modeling evaluation. Powder Technol 217:558–565

[89] Knowles AJ, Jiang X, Galano M, Audebert F (2014) Microstructure and mechanical properties of 6061 Al alloy based composites with SiC nanoparticles. J Alloys Compd 615:S401–S405

[90] Poovazhagan L, Kalaichelvan K, Rajadurai A, Senthilvelan V (2013) Characterization of hybrid silicon carbide and boron carbide nanoparticles-reinforced aluminum alloy composites. Procedia Eng. 64:681–689

[91] Akbari MK, Mirzaee O, Baharvandi HR (2013) Fabrication and study on mechanical properties and fracture behavior of nanometric Al_2O_3 particle-reinforced A356 composites focusing on the parameters of vortex method. Mater Des 46:199–205

[92] Mazahery A, Abdizadeh H, Baharvandi HR (2009) Development of high-performance A356/nano- Al_2O_3 composites. Mater Sci Eng A 518(1):61–64

[93] Ezatpour HR, Sajjadi SA, Sabzevar MH, Huang Y (2014) Investigation of microstructure and mechanical properties of Al6061-nanocomposite fabricated by stir casting. Mater Des 55:921–928

[94] Fine ME (1975) Precipitation hardening of aluminum alloys. Metall Trans A 6(4):625

[95] Song M, He YH, Wu ZG, Huang BY (2009) Multi-scale model for the ductility of multiple phase materials. Mech Mater 41(5):622–633

[96] Song M, Huang D (2007) Experimental and modeling of the coupled influences of variously sized particles on the tensile ductility of SiC_p/Al metal matrix composites. Metall Mater Trans A 38(9):2127–2137

[97] Kallip K, Babu NK, Alogab KA, Kollo L, Maeder X, Arroyo Y, Leparoux M (2017) Microstructure and mechanical properties of near net shaped aluminum/alumina nanocomposites fabricated by powder metallurgy. J Alloys Compd 714:133–143

[98] Kumar GSP, Koppad PG, Keshavamurthy R, Alipour M (2017) Microstructure and mechanical behavior of in situ fabricated AA6061-TiC metal matrix composites. Arch Civ Mech Eng 17:535–544

[99] Li M, Ma K, Jiang L, Yang H, Lavernia EJ, Zhang L, Schoenung JM (2016) Synthesis and mechanical behavior of nanostructured Al 5083/n-TiB_2 metal matrix composites. Mater Sci Eng A 656:241–248

[100] Jiang L, Yang H, Yee JK, Mo X, Topping T, Lavernia EJ, Schoenung JM (2016) Toughening of aluminum matrix nanocomposites via spatial arrays of boron carbide spherical nanoparticles. Act Mater. 103:128–140